Projected Changes in Extreme Rainfall in New Jersey based on an Ensemble of Downscaled Climate Model Projections

Art DeGaetano

Northeast Regional Climate Center

Department of Earth and Atmospheric Science

Cornell University, Ithaca NY

Abstract

Projections from 46 downscaled climate model simulations were used to project the change in magnitude of extreme rainfall events used in engineering design and planning. A methodology analogous to that used in NOAA Atlas 14 was used to calculate annual average return period precipitation amounts from the model data to allow the computation of future change factors that can be applied to the Atlas 14 precipitation data to simulate future extreme rainfall conditions.

Across the state the calculated change factors (CF) are >1 indicating an increase in extreme precipitation amounts. In general, CF values are larger in the northern part of New Jersey and smaller in central NJ and along the coast. Under a high RCP8.5 emissions median CF values range from between 1.10 and 1.30 by the end of the century, indicating a 10-30% increase in extreme precipitation amounts. Under more moderate RCP4.5 emissions, the CFs for 2- and 10-yr annual recurrence interval (ARI) precipitation amounts by the end of the century are typically 1.05-1.15. The CF for 100-yr ARI are more variable ranging from little change (i.e. CF = 1.00) in the vicinity of New York City to larger 20-25% increases in northern NJ.

1. Introduction

Intensity-Duration-Frequency (IDF) curves summarize the relationship between extreme rainfall intensity, duration and average recurrence interval or frequency of exceedance. This relationship is based on statistical analysis of long historical rainfall records. NOAA Atlas 14, published in volumes covering different parts of the U.S. (Bonnin et al. 2006; Perica et al. 2014) provides the foundation for such extreme rainfall analyses in New Jersey and the United States. A key assumption in the development of Atlas14 has been that the rainfall record is stationary. This infers that past rainfall observations reflect conditions that are likely in the future. The validity of this assumption has been called into question resulting in concern that IDF curves that rely on past observations may not be an adequate guide under future climate conditions (Yan et al. 2020).

New Jersey and much of the mid-Atlantic region of the United States has exhibited notable increases in extreme precipitation. For example, this region has experienced a greater than 70% increase in the heaviest 1% of daily precipitation events over the period 1958-2010, which represents the highest regional increase in the US (Groisman et al. 2012, Kunkel et al. 2013, Walsh et al. 2014). In addition, parts of the region have also experienced a documented increase in flooding and rainfall events that are conducive to flooding, especially in urban environments (Collins 2009, DeGaetano 2009, Armstrong et al. 2014, Peterson et al. 2013, Georgakakos et al. 2014). The Mid-Atlantic U.S. is not the only region that has been experiencing greater extreme precipitation frequency and magnitude. Similar trends are noted in the central and southeastern US (Groisman et al. 2012, Cooley and Chang 2017, Brown et al. 2020) as well as many other regions throughout the world (Groisman et al. 2005, Fisher and Knutti 2016, Lenderink et al. 2011).

Coumou and Rahmstorf (2012) point to increases in atmospheric water vapor (consistent with increasing average temperature) and increases in the frequency of local convective storm events (also enhanced by warming surface temperatures) as physical reasons for these changes. In addition, changes in frequency, intensity, and tracks of tropical and extra-tropical cyclones contribute to trends in extreme precipitation (Kunkel et al., 2010). In some cases, linkages to certain atmospheric circulation patterns have been posed as influencing changes in precipitation extremes (e.g. Kenyon and Hegerl, 2010). Climate model simulations suggest a continuation of these extreme precipitation trends through the 21st century (e.g. Donat et al. 2016; Ning et al. 2015; Sun et al. 2016). While the existence of trends in historical observations does not guarantee trends in future events, the prominence of the extreme precipitation trend, especially in combination with the consistency in the sign of model projections for extreme precipitation, is highly suggestive of future increases and sets a minimum level of what is physically possible.

The significant increases in extreme precipitation since the mid-to-late 20th century noted in the climate record (DeGaetano, 2009; Groisman, 1992; Heineman, 2012; Kunkel et al., 1999; Kunkel, 2003) have raised practical concerns about use of an assumed stationary historical record to design infrastructure with a lifetime that extends well into the future. For example, DeGaetano (2009) reports that rainfall amounts once considered 1-in-100-year events based on the data record available from 1950-1978, occur as often as once every 60 years based on data observed across the Northeast from 1978-2007. This problem is exacerbated by climate model projections suggesting that the frequency and magnitude of extreme precipitation will continue to increase throughout the twenty-first century (e.g., DeGaetano and Castellano, 2017).

Two broad approaches have been used to account for the non-stationarity of the rainfall record when assessing rainfall extremes. The first attempts to estimate the trend either in the

rainfall itself or potential drivers of the rainfall change and project this trend into the future. The resulting IDF curves are dependent on the selected variable (e.g., time) (Agilan and Umamahesh 2017; Cheng and AghaKouchak 2014; Sarhadi and Soulis 2017). In the second approach, climate projections from Global Climate Models (GCM) are used to construct future IDF curves. These are often based on different greenhouse gas emissions scenarios (Cook, Anderson, and Samaras 2017; DeGaetano and Castellano 2017; Ragno et al. 2018; Wu et al. 2019). Although both approaches have been used in practice, each has advantages and disadvantages.

The construction of time-dependent IDF curves requires long historical rainfall observations in order to establish the existence and magnitude of a time-dependent trend. The record must also be free of any non-climatic influences such as changes in instrumentation or station siting. Wright et al. (2019) show that quantifying station-scale nonstationary in precipitation frequency estimates with confidence is often unattainable. GCM projections are associated with their own biases and typically are only available at coarse resolution. Downscaling methods provide an approach to refine the resolution of GCM output to a scale more conducive to assessing local impacts. However, a wide range of methodologies exist complicating analyses.

Previous work has implemented both methods either independently or in combination (e.g. DeGaetano and Castellano 2017; Ragno et al. 2018; Wu et al. 2019). Despite these differences in methodology, it is useful to compare the results of these related studies. Ragno et al. (2018) used a combination of trend analysis and multi-model downscaled simulations to assess future IDF curves at the city scale. They found a 10% increase in 25-, 50- and 100-year ARI precipitation was indicated in the 2050-2099 period in New York City under high RCP8.5 emissions. A similar albeit smaller increase was found to occur in Washington, DC Ragno et al.

(2018).   An alternative study (Wu et al. 2019), used downscaled GCM projections and concluded that on average across the Northeast ensemble mean rainfall extremes will increase by 22% in the 2054-2100 period under high RCP8.5 emissions and by 12% under moderate RCP 4.5 emissions.

DeGaetano and Castellano (2017) used a suite of GCM models and downscaling approaches to develop future IDF curves for the state of New York. There were considerable differences in the projected changes in rainfall extremes between these different downscaling methodologies and climate models given difference in the base models' resolution, parameterizations of convective and rainfall generation processes and non-systematic biases in the downscaling approaches. Spatial and between model variability was largest for the NA-CORDEX simulations compared to the other methods. Across all GCM-downscaling method combinations, the 100-year ARI precipitation amount in 2070-2099 increased by between 15% and 25% statewide, under RCP 8.5.

Building from DeGaetano and Castellano (2017) and other previous work, the most up-to-date global climate change model projections and state-of-the-art downscaling methods, are used to develop climate change-informed ARI precipitation values that can be applied in New Jersey to plan and design for anticipated future precipitation conditions. The approach is rooted in the methodology conventionally used to analyze historical extreme precipitation records but extends this common practice to data from available climate model projections and downscaling techniques.

A change-factor approach was used to align with similar work done in surrounding states (Miro et al., 2021) and to facilitate use with Atlas 14. This report details the data (section 2) and methods (section 3) used to project future 1-day rainfall extremes in two future time periods

(2020-2070 and 2050-2100). The results, including an assessment of model biases in the 1950-1999 historical period, change factors for the individual models and downscaling techniques included in the ensemble of methods evaluated, and final projections synthesizing information from more than 40 model-downscaling technique combinations are presented in Section 4. Results are presented for 2-, 10- and 100-year ARI precipitation under RCP 4.5 (moderate emissions) and RCP 8.5 (high emissions) Data are also available for 5-, 25- and 50-year ARI rainfall.

2. Data

i. Downscaled climate model datasets

Historical and future downscaled atmosphere–ocean general circulation model (AOGCM) and Earth System model (ESM) output was obtained from four sources 1) North American Coordinated Regional Downscaling Experiment (NA-CORDEX) (Mearns et al., 2017), Bias Corrected Constructed Analogue (BCCAv2) (Maraun et al., 2010), Localized Constructed Analog (LOCA) (Pierce et al., 2014), and Multivariate Adaptive Constructed Analogs (MACA) (Abatzoglou and Brown, 2012). Simulations from the models' historical period and two future Representative Concentration Pathways (RCP4.5 and RCP 8.5) (Collins et al. 2013) were used. Table 1 highlights the unique features of each of these datasets. For example, LOCA downscaling provides one of the highest resolution outputs, while NA-CORDEX, the only dynamically downscaled dataset selected for this study, has a much coarser spatial resolution. Since the downscaling approach, choice of global climate model (GCM) and RCP, and spatial and temporal resolution each introduce their own source of uncertainty, it is important to consider a range of these features to capture the plausible range of future precipitation extremes.

The ability of each of these downscaled datasets in simulating extreme precipitation was evaluated by Lopez-Cantu et al. (2020). They found substantial differences among the datasets in both the magnitude and spatial pattern of projected extreme precipitation. These differences

Table 1. Characteristics of downscaled climate model datasets evaluated in this study

Dataset	RCPs	Approximate gridded spatial resolution*	Temporal resolution	Downscaling approach
BCCAv2	4.5,8.5	12 km (7.5 miles)	Daily	Statistical
MACA	4.5, 8.5	4 km (2.5 miles)	Daily	Statistical
LOCA	4.5, 8.5	6 km (3.7 miles)	Daily	Statistical
NA-CORDEX	8.5	25 km (15.5 miles)	Daily and Sub-daily	Dynamical
NA-CORDEX	4.5	25 km (15.5 miles)	Daily	Dynamical
NA-CORDEX	4.5	50 km (31 miles)	Daily	Dynamical

*Gridded spatial resolutions across all datasets are approximate and based on conversions from degrees to kilometers at mid-latitudes.

are likely due to the downscaling methodology as opposed to differences in the choice of model or spatial resolution. Historical (1951-2005) MACA simulations exhibited the least bias when compared to observed rainfall data, while BCCA simulations consistently underestimated the observed values. In terms of future (2044-2099) projections, the change in extreme rainfall given by MACA was considerably larger than that of the other models. Conversely the BCCA future projections exhibited the smallest change. When compared to the projected changes in the native-resolution GCM, both the MACA and BCCA projections diverged from the original GCM signal, with BCCA mostly lower and MACA substantially higher (Lopez-Cantu et al., 2020). These differences were found to be related to the methodological choices within the downscaling procedures rather than the selected GCMs. Although it is possible for dynamical downscaling methods to alter the driving GCM signal given their incorporation of improved surface representation and capability to solve physical processes at higher resolution, in statistical

methods, such as those used in MACA and BCCA, such difference are likely the result of signal artifacts associated with the very low frequency of occurrence of the events being simulated (Eum & Cannon, 2017; Lopez-Cantu et al., 2020). Given this behavior, especially when coupled with the underestimation identified in the BCAA data, Lopez-Cantu et al. (2020) urged caution in the use of these data sets. Thus, these data sources were excluded from the final analyses.

The LOCA dataset is widely used, as it forms the basis for downscaling in the current National Climate Assessment (USGCRP, 2018). Projections from the 31 GCMs summarized in Table 2, downscaled to a spatial resolution of 0.0625° (approximately 6 km or the distance from Philadelphia to Camden), provide the foundation for the LOCA dataset. The LOCA data cover a 1950-2005 historical period and projections for the 2006-2099 future period using RCP4.5 and RCP8.5. Details regarding the statistical downscaling methodology used in LOCA can be found in (Pierce et al., 2014). Briefly, the method begins by matching the spatial pattern of the variable of interest from a future GCM projection to that based on historical observations over a region. From a pool of candidate observed historical analog days the single best candidate, based on minimization of root mean square error, is chosen as an analog, unless a different analog day is selected for neighboring grid cells, in which case a weighted combination of the observed analog days is used. In either case, high-resolution observed data corresponding to the historical analog day is used to represent the downscaled future rainfall.

NA-CORDEX, on the other hand, employs a dynamical downscaling approach based on a set of regional climate models (RCM) with boundary conditions specified by GCM simulations from the CMIP5 archive. The RCM domain is limited to the area covering the majority of North America. Like LOCA, historical and future simulations are available for the period 1950-2100,

using both RCP8.5 and RCP4.5. Most simulations are available with a spatial resolution of 0.22°

(approximately 25 km or the distance from Woodbridge to Newark), however a subset of

RCP4.5 simulations are only available at a 0.44° (50 km) resolution. While all CORDEX

simulations are available at a daily temporal resolution, a limited number of simulations provide

output at either 3-hourly or hourly resolution. Table 3 summarizes the NA-CORDEX

simulations used.

Table 2 List of CMIP5 models used in LOCA downscaling

ID	Model	Modeling Center/Group	Resolution
1	ACCESS1.0	CSIRO, Australia	1.25° × 1.875°
2	ACCESS1.3	CSIRO, Australia	1.25° × 1.875°
3	CCSM4	National Center for Atmos. Research (NCAR), USA	0.9° × 1.25°
4	CESM1-CAM5	Community Earth System Model, NCAR, USA	0.9424° × 1.25°
5	CMCC−CM	Euro−Mediterranean Centre on Climate Change, Italy	0.75° × 0.75°
6	CMCC−CMS	Euro−Mediterranean Centre on Climate Change, Italy	3.7111° × 3.75
7	CNRM−CM5	National Centre for Meteorological Research, France	1.4° × 1.4°
8	CSIRO−Mk3.6.0	CSIRO, Australia	1.875° × 1.875°
9	CanESM2	Canadian Centre for Climate Modeling and Analysis, Canada	1.875° × 1.875°
10	EC-EARTH	EC Earth Consortium	1.1215° x 1.125°
11	FGOALS−g2	LASG, China	2.8° × 2.8°
12	GFDL−CM3	Geophysical Fluid Dynamics Lab, USA	2.0° × 2.5°
13	GFDL−ESM2**M**	Geophysical Fluid Dynamics Lab, USA	2.0° × 2.5°
14	GFDL−ESM2**G**	Geophysical Fluid Dynamics Lab, USA	2.0° × 2.5°
15	GISS−E2−H	NASA Goddard Inst. for Space Sci., USA	2.0° × 2.5°
16	GISS−E2−R	NASA Goddard Inst for Space Sci, USA	2.0° × 2.5°
17	HADGEM2−AO	Met Office Hadley Centre, United Kingdom	1.25° × 1.875°
18	HADGEM2−CC	Met Office Hadley Centre, United Kingdom	1.25° × 1.875°
19	IPSL−CM5A−MR	Pierre Simon Laplace Institute, France	1.25° × 2.5°
20	IPSL−CM5**A**−LR	Pierre Simon Laplace Institute, France	1.9° × 3.75°
21	MIROC−ESM	JAMSTEC/AORI/NIES, Japan	2.8° × 2.8°
22	MIROC−ESM−CHEM	JAMSTEC/AORI/NIES, Japan	2.8° × 2.8°
23	MIROC5	JAMSTEC/AORI/NIES, Japan	1.4° × 1.4°
24	MPI-ESM-**M**R	Max Planck Inst. For Meteorol., Germany	1.8653° x 1.875
25	MPI-ESM-**L**R	Max Planck Inst. For Meteorol., Germany	1.8653° x 1.875
26	MRI−CGCM3	Meteorological Research Institute, Japan	1.125° × 1.125°
27	NorESM1−M	Norwegian Climate Center, Norway	1.9° × 2.5°
28	BCC−CSM1.1	Beijing Climate Center, China	1.125° × 1.125°
29	BCC−CSM1.1(m)	Beijing Climate Center, China	2.8° × 2.8°
30	BNU−ESM	Beijing Normal University, China	2.8° × 2.8°
31	inmcm4*	Inst. of Numerical Mathematics, Russian Academy of Sciences	1.5° × 2.0°

*projection only

Table 3. NA-CORDEX simulations used in this study

ID	Global Scale Model	Regional Climate Model*	Spatial Resolution (units)	Temporal Resolution	RCP
1	CanESM2	CRCM4[b]	22	daily	8.5
2	CanESM2	CRCM5-OUR [b]	22	daily	8.5
3	CanESM2	CRCM5-UQAM [b]	22	daily	8.5
4	CNRM-CM5	CRCM5-OUR [b]	22	daily	8.5
5	GEMatm-Can*	CRCM5-UQAM [b]	22	daily	8.5
6	GEMatm-MPI*	CRCM5-UQAM [b]	22	daily	8.5
7	GFDL-ESM2M	CRCM5-OUR [b]	22	daily	8.5
8	GFDL-ESM2M	RegCM4[a]	22	daily 3-hr	8.5
9	GFDL-ESM2M	WRF[e]	22	daily 1-hr	8.5
10	HadGEM2-ES	RegCM4 [a]	22	daily 3-hr	8.5
11	HadGEM2-ES	WRF[e]	22	daily 1-hr	8.5
12	MPI-ESM-LR	CRCM5-OUR	22	daily	8.5
13	MPI-ESM-LR	CRCM5-UQAM	22	daily	8.5
14	MPI-ESM-LR	RegCM4 [a]	22	daily 1-hr	8.5
15	MPI-ESM-LR	WRF[e]	22	daily 1-hr	8.5
16	MPI-ESM-MR	CRCM5-UQAM	22	daily	8.5
1	CanESM2	CRCM4 [b]	44	daily	4.5
2	CanESM2	CRCM5-UQAM [b]	44	daily	4.5
3	CanESM2	RCA4[c]	22	daily	4.5
4	EC-EARTH	HIRAM5[d]	22	daily	4.5
5	EC-EARTH	RCA4 [c]	22	daily	4.5
6	MPI-ESM-LR	CRCM5-UQAM [b]	44	daily	4.5
7	CanESM2	CRCM4 [b]	22	daily	4.5
8	CanESM2	CRCM5-OUR [b]	22	daily	4.5
9	GFDL-ESM2M	CRCM5-OUR [b]	22	daily	4.5

*GEMatm is a global version of the CRCM5 regional model (Hernandez-Diaz, 2019)

[a]RegCM4: Regional Climate Model System, National Center for Atmospheric Research, USA

[b]CRCM4 and CRCM5 Canadian Regional Climate Model, Canadian Centre for Climate Modeling and Analysis, Canada*. Complementary Simulations available from Université du Québec à Montréal (UQAM)and OURANOS, Canada.

[c]RCA4: Rossby Centre regional climate model, Rosby Centre, Sweden

[d]HIRAM5 High Resolution Atmospheric Model, Geophysical Fluid Dynamics Lab, USA

[e]WRF: Weather Research and Forecasting Model National Center for Atmospheric Research, and others, USA

A limited set of results using GCM scale sub-daily simulations from the new CMIP6 data archive were also examined. This next evolution of the Coupled Model Intercomparison Project Phase is ongoing. Downscaled datasets based on CMIP6 simulations are not yet available.

ii Station Data

The downscaled climate model simulations for the historical period were compared to the ARI precipitation amounts from a set of 55 stations with records spanning the period from 1950-2019. These stations corresponded to those analyzed in a companion report investing changes in ARI precipitation since the publication of NOAA Atlas 14. The stations are a part of the NOAA Cooperative Observer Network and were selected based on 1) their location within a region extending from 41.7°N to 37.5°N and 76.0°W to 72.5°W , 2) inclusion in NOAA Atlas 14 Volume 2 or Volume 10 (Bonnin et al., 2006; Perica et al., 2019) and 3) less than 5% of daily precipitation missing in the 2050-2019 period. Similarly, a larger set of regional stations was retained that included these base stations and additional sites meeting the above selection criteria, buts having at least 20 years of record after 1980. For all sites, daily rainfall observations and flags were extracted from the Applied Climate Information System (ACIS) and reflect the values in the GHCN on January13, 2021. Station data were analyzed using a method analogous to that used to compute ARIs for the downscaled climate model projections that is described in the next section.

3. Methods

Once the relevant data sets were downloaded, data processing proceeded according to the steps described below and outlined in Figure 1.
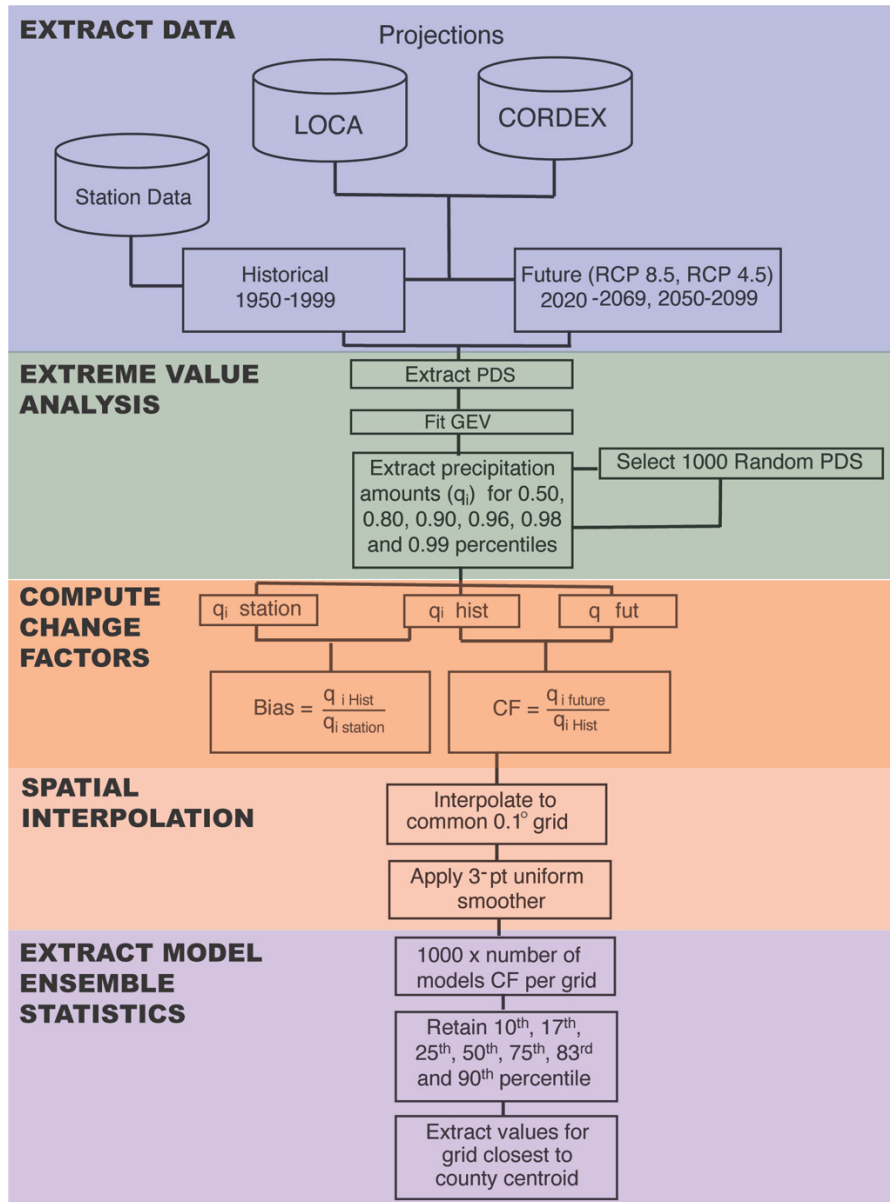
Figure 1. *Workflow to analyze gridded downscaled climate projections and estimate change factors at the county scale for the study area. The same workflow was repeated for each future period and RCP scenario.*

i. Extreme value analysis

Extreme rainfall events were extracted separately from each downscaled data set and model. Conventionally, extreme rainfall analyses have been based on either annual maximum series (AMS) or partial duration series (PDS) (Madsen et al., 1997). Using AMS, the largest

precipitation event for a specific duration is selected for each year. This potentially omits some

independent large precipitations, as only a single event can be assigned to each year. Thus, if

extreme rainfall associated with two distinct hurricanes impacts a location in the same year, only

the rainfall from one can be considered. Using PDS, the *n* largest independent precipitation

events are extracted, where *n* represents the number of available years of record. Thus, two

events can be selected from the same year, provided they do not occur within seven days of each

other. This 7-day period is chosen to assure the independence between the events. PDS are used

as the basis of this work, given this method's widespread application (e.g. Cook et al., 2017;

DeGaetano and Castellano 2017; Lopez-Cantu et al., 2020; Ragno et al. 2018; Thakali et al.,

2016; Wu et al. 2019) and to ensure the inclusion of all relevant extreme rainfall events projected

in the downscaled climate simulations. Figure 2 shows the difference in the AMS and PDS from

a downscaled GCM gridpoint near Newark, NJ. It is apparent that several large precipitation

events would be excluded using the AMS. All PDS events exceed 2 inches, whereas several

AMS events, are associated with < 2 inch daily precipitation amounts.
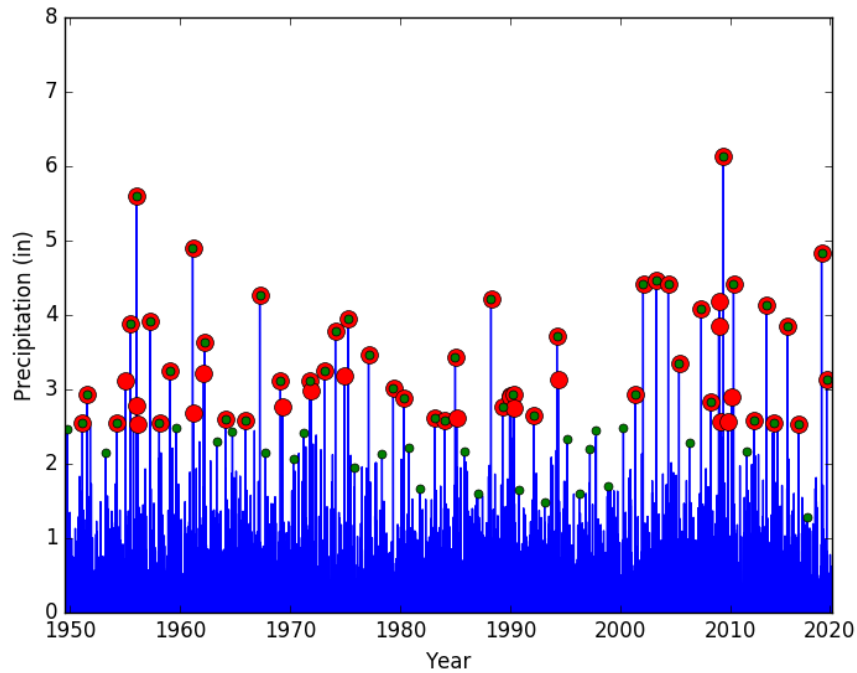
Figure 2. *Time series of LOCA model downscaled daily precipitation for a grid point near Newark, NJ. The PDS events are highlighted by red dots. AMS events are shown by the smaller green dots.*

A PDS was compiled for each grid cell, corresponding to the 50-year period from 1950-1999. This period was designated the historical period as it corresponds to each downscaled model's historical simulation period. Likewise, this time-period corresponds to the longest available overlap period between the downscaled simulations and stations included in NOAA Atlas 14. PDS for two future time periods 2020-2069 and 2050-2099 were also extracted. The 50-year length was selected to assure an adequate sample size for extreme value analysis, and to minimize the influence of the non-stationarity of the record and the potential effect of natural interdecadal variations in the extreme rainfall record (DeGaetano and Castellano, 2020). Separate PDS were also compiled for simulations using RCP8.5 and RCP4.5.

16

For each PDS, rainfall amounts corresponding to recurrence probabilities of 50%, 20%, 10%, 4%, 2% and 1% (i.e. 2-, 5-, 10- 25-, 50- and 100-year storms) were computed by simulating the methodology used in NOAA Atlas 14 (Bonnin et al., 2006; Perica et al., 2019). First, the python lmoments package (https://pypi.org/project/lmoments/) was used to fit the generalized extreme value (GEV) distribution to each grid point's PDS using the methods of Hosking (1990). Although not the only valid theoretical distribution for estimating extreme rainfall probabilities, the use of the GEV has been standard practice in prior extreme rainfall analyses (e.g. Papalexiou and Koutsoyiannis, 2013). Given the L-moments estimates for the GEV parameters, the lmoments library quagev method was used to obtain the specified quantiles of the GEV distribution.

In addition, the regional L-moments procedure used in NOAA Atlas 14 Volume 10 (Perica et al., 2019) was adapted. Although the majority of sites lied outside the region covered by this atlas, the methodology employed to develop regions in the later atlas was an improvement over the earlier implementation as it defined regions relative to each station rather than a small set of broad regions and corrected an error in the procedure used to define confidence intervals. For each grid point, the 20 closest neighboring grids points, were identified. Sample lmoments were obtained for each of these points using the lmoments library samlmu routine and an average of the higher order moments computed. These averages along with the base grid's location parameter (i.e. mean) were then used to obtain GEV parameters and quantiles.

In separate work, two other fitting methods, the Maximum Likelihood Estimator (MLE) and the Generalized Maximum Likelihood Estimator (GMLE) that have been used in similar analyses (Martins and Stedinger, 2000) were compared. The MLE and GMLE methods have

fundamentally the same objective (to maximize the log-likelihood function), but they differ in the sense that GMLE introduces a prior distribution for the shape parameter, limiting it to a physically credible interval. The R library *extRemes* was used to perform both the MLE and GMLE fit on each PDS series. The Akaike Information Criterion (AIC) was then used to compare the MLE and GMLE methods. AIC has been used in previous analyses to compare extreme models. While the GMLE method outperformed the MLE approach, there was not a clear advantage to using the method instead of the L-moments approach. Thus, to align with NOAA Atlas 14 and to avoid the prior assumptions about the shape parameter required by the GMLE method, L-moments fitting was adopted in this work.

ii. Change factor definition

As outlined in Figure 2, the development of 2-, 5-, 10-, 25-, 50- and 100-year recurrence interval precipitation amounts using L-moments fitting of the GEV distribution is the second of a five-part workflow. In the third step an ensemble of change-factors were computed for each gridpoint-model-RCP combination. Change-factors (CF) are defined as:

$$CF_i = \frac{P_{i,r,future}}{P_{r,historical}}$$

Where P is the precipitation associated with i^{th} ensemble member for the rth recurrence interval computed for either one of the two *future* periods (2020-2069 or 2050-2099) or the 1950-1999 *historical* period. Ultimately the CFs computed using values obtained from single station versus regional L-moments fitting were similar. The regional approach, however, was adopted to

simulate the Atlas 14 methodology and since these values tended to be less variable from point to point.

For each grid-model-RCP combination an ensemble (*i*) of 1000 simulations was also constructed via a resampling procedure. From the GEV distribution fit to the original downscaled future period PDS, 1000 50-member PDS were randomly selected using the scipy genextreme rvs function. A new GEV distribution was fit to each random PDS, retaining the original regional average of the higher order moments, and the resulting 2-, 5-, 10-, 25-, 50- and 100-year recurrence interval precipitation amounts used to compute 1000 random CF.

iii Spatial interpolation and smoothing

Next, the CF values were interpolated to a common 0.1° grid to allow the results from the different downscaling methods to be combined. The scipy.interpolate griddata function was used to perform nearest neighbor interpolation. Finally, to smooth the spatial variations which often existed between neighboring grid points a 3-point uniform smoothing (i.e. the average of the grid and its two closest neighbors in each direction) was applied using the sci ndimage uniform_filter function. The interpolate griddata function was also used to interpolate the CF from the 0.1 grid to county centroids. Given the lack of spatial variation in CF, the county-level values obtained via this approach were not substantially different from those that would have resulted if a weighted average of grids encompassing a county were used.

iv. Quantification of uncertainty

In the final step, the uncertainty of the CFs was quantified. At each 0.1° grid point an ensemble of 47,000 CFs was available for each recurrence interval under RCP8.5 (47 models; 31

LOCA and 16 CORDEX x 1000 resamples) and 40,000 CFs existed under RCP4.5. From this

ensemble the median CF factor was obtained as were the 17th, 25th, 75th and 83rd percentiles. The

17th and 83rd percentiles were selected to represent a likely range (Mastrandrea et al. 2010) of

projections around the median.

4. Results

i. Station Bias

   Station biases were computed by comparing the observed ARI precipitation at each station

with the analogous value computed based on each model's historical period downscaled

precipitation from the closest grid point. Bias is expressed as a ratio (model divided by station).

Thus, bias values >1 indicate the downscaled simulation overestimates the observed values,

while bias < 1 indicates underestimation by the downscaled data. Biases are presented for 2- 10-

and 100- year ARI rainfall in Figures (3-11). In each figure, the mapped values show the median

bias across all models at each station. Boxplots show the bias of individual models across all

stations.

a. LOCA

   The LOCA projections underestimated the 2-, 10- and 100-year ARI precipitation at the

majority of stations. Model-to-model differences in the median bias for 2-yr ARI precipitation

across all stations ranged from 65 to 80% of the observed values (Fig. 3). At specific stations, the

model-median biases ranged from <60 to >100%, with the median (and mean) bias across all

models and stations near 70%. There was only some indication of a spatial pattern to the model-

median bias, with inland stations experiencing smaller biases (or even overestimates) and larger

negative biases at coastal locations. Similar bias magnitudes and model-to-model variations were

also noted for both 10-yr and 100-yr ARI precipitation (Fig. 4 and Fig. 5). Likewise, biases were

closer to 1.0 at inland locations, with underestimates of 10- and 100-yr ARI precipitation prevalent at coast stations.
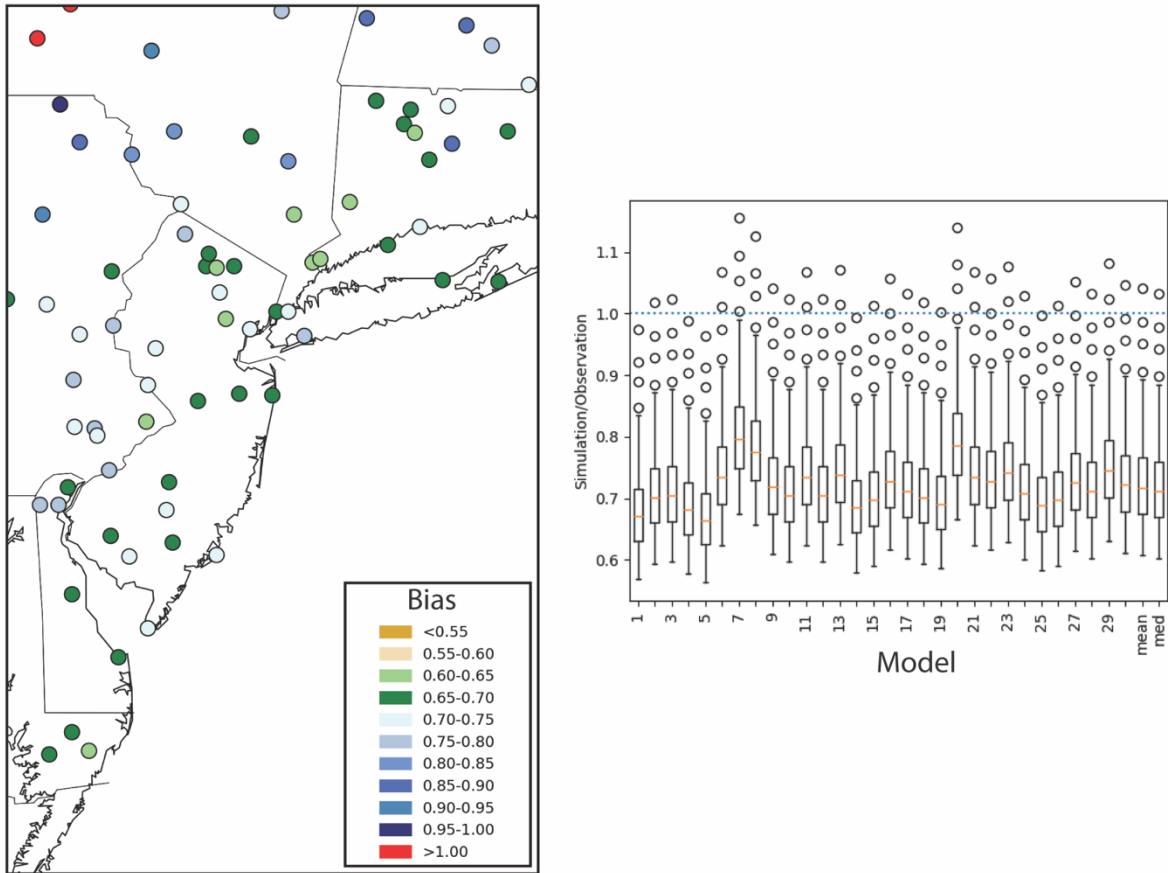

Figure 3. Bias associated with LOCA model simulations of 2-yr ARI precipitation for the 1950-1999 historical period. In the map, the 30-model LOCA median is shown for each station. The boxplots show the bias for each model (numbers correspond to models listed in Table 2) across all stations. Model 31 (inmcm4) is excluded since a historical simulation is not available for this model.
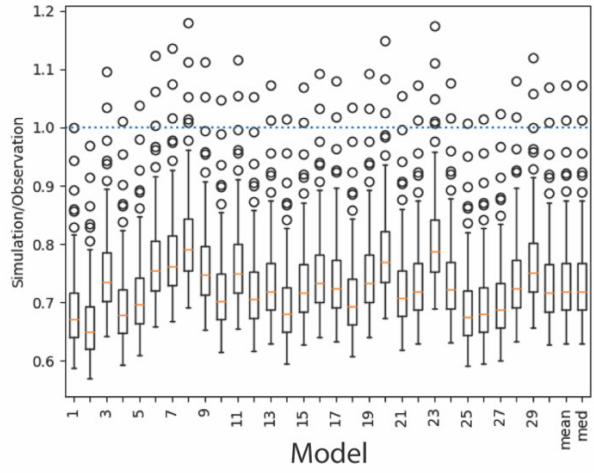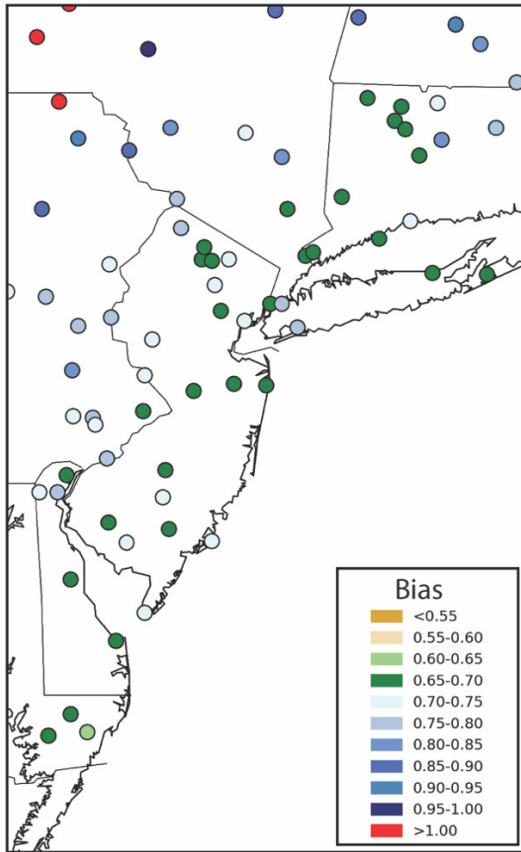
Figure 4. As in Figure 3, but for 10-yr ARI precipitation.
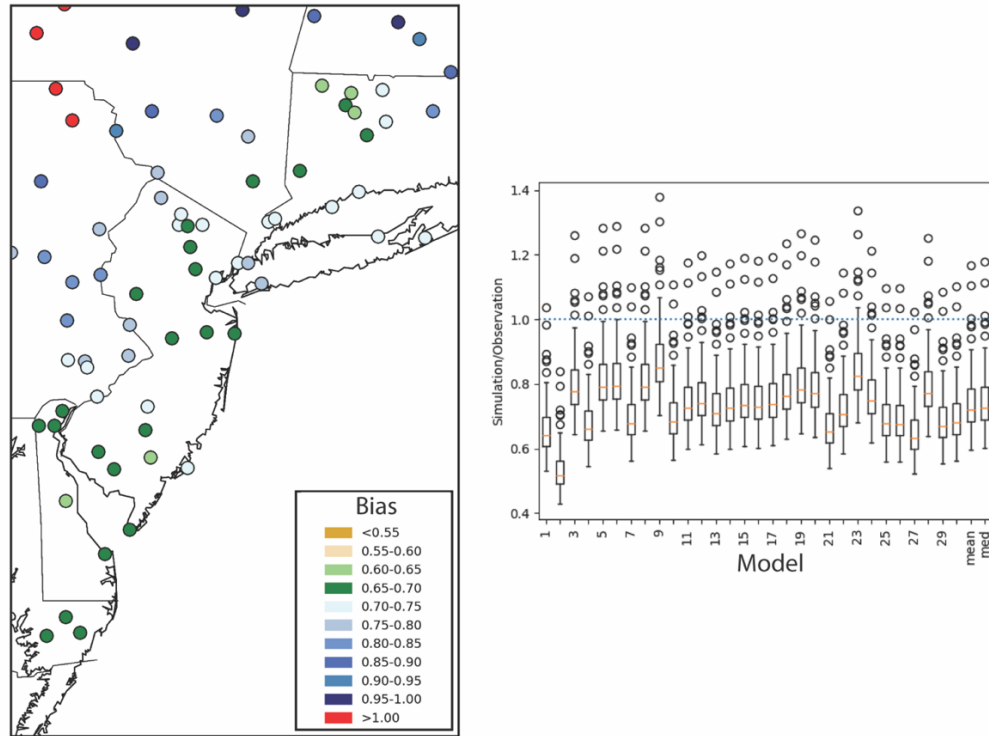
Figure 5. As in Figure 3, but for 100-yr ARI precipitation.

b. *CORDEX RCP 8.5*

Unlike the LOCA simulations, the CORDEX models generally overestimated the observed 2-yr ARI precipitation and displayed a much larger degree of model-to-model variation. Model-to-model differences in the median bias for 2-yr ARI precipitation across all stations ranged from 90 to 130% of the observed values (Fig. 6). At specific stations, the model-median biases ranged from 90 to over 140%, with the median (and mean) bias across all models and stations near 110%. The inland versus coastal pattern of bias noted for the LOCA projections was not apparent. For example, stations with biases in the 120-125% range were located at Cape May, NJ and Lewes, DE; JFK Airport; and stations in northeastern Pennsylvania (Fig 6). The model-median bias at neighboring stations in southern NJ varied considerably. For some models, the

median overestimation exceeded 30%, while others underestimated the 2-yr ARI rainfall by 10% (Fig. 6).

For 10-yr ARI, the median (and mean) bias across all models and stations decreased to near 100% (Fig. 7). However, model-to-model differences in the median bias across all stations remained large, ranging from 85 to 125% of the observed values (Fig. 7). Some models underestimated observed 10-yr ARI precipitation by as much as 40%, while others overestimated this value by more than 60% (Fig. 7). Like the 2-yr ARI, there was not a clear spatial pattern of model-median bias. In some cases, the median model simulations were 70% of the station values. This level of bias approached that for the LOCA simulations.

Median (and mean) bias across all models and stations became <1.0 for 100-yr ARI precipitation indicating a change from primarily overestimation by the CORDEX models to underestimation. Model-to-model differences in the median bias across all stations remained large, ranging from < 80% for five models to over 120% in one case. At four stations, the ACCESS1.0 model overestimated the 100-yr ARI by more than 60%. The pattern of greater underestimation near the coast as opposed to inland which was characteristic of the LOCA model is somewhat more evident for the CORDEX 100-yr ARI values.
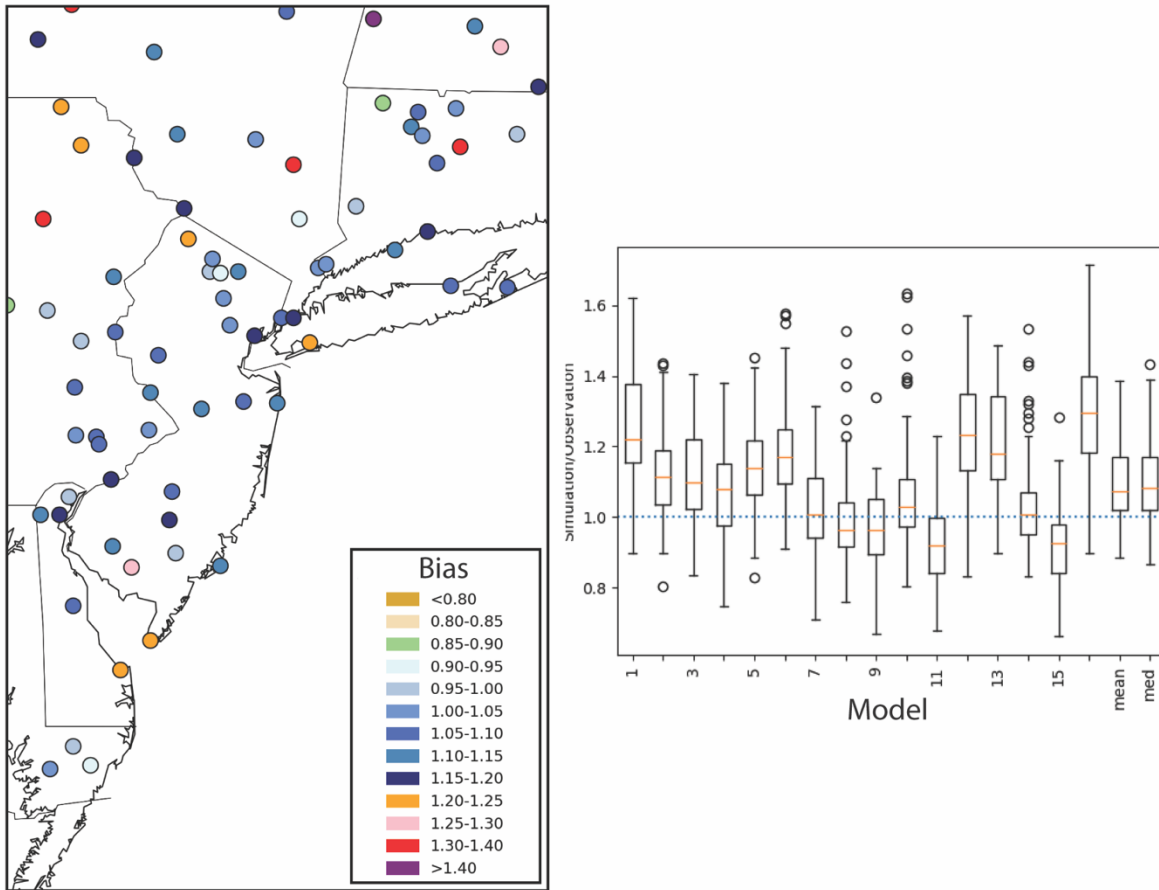
Figure 6. Bias associated with CORDEX RCP8.5 model simulations of 2-yr ARI precipitation for the 1950-1999 historical period. In the map, the 16-model CORDEX median is shown for each station. The boxplots show the bias for each model (numbers correspond to models listed in Table 3) across all stations.
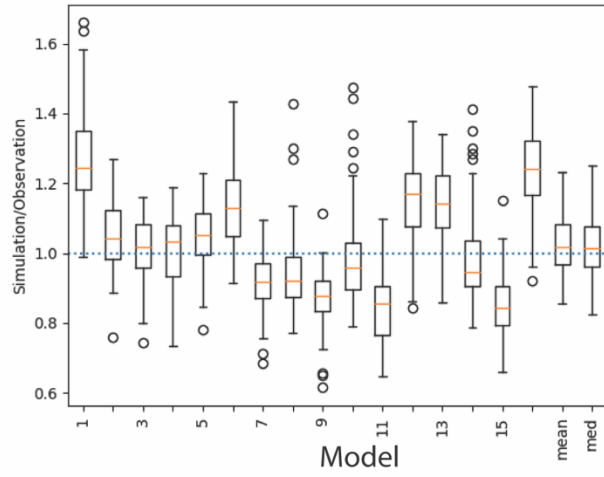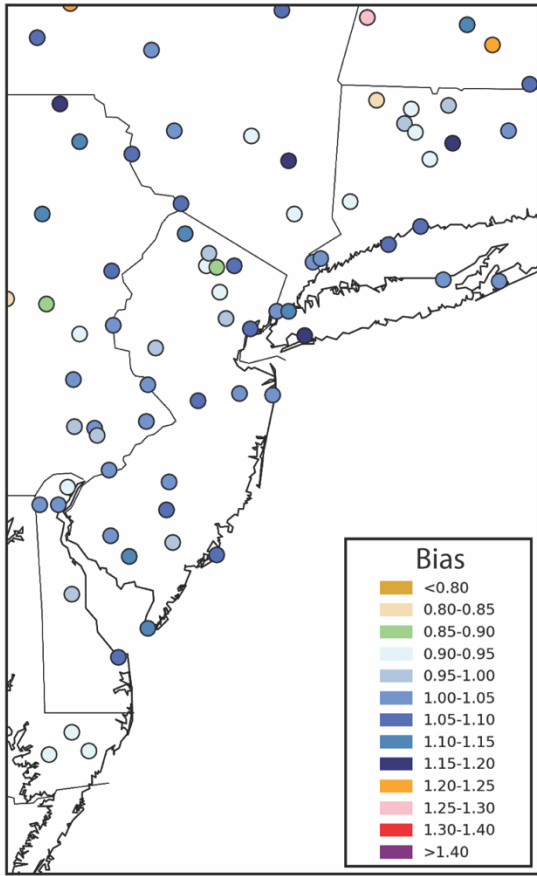
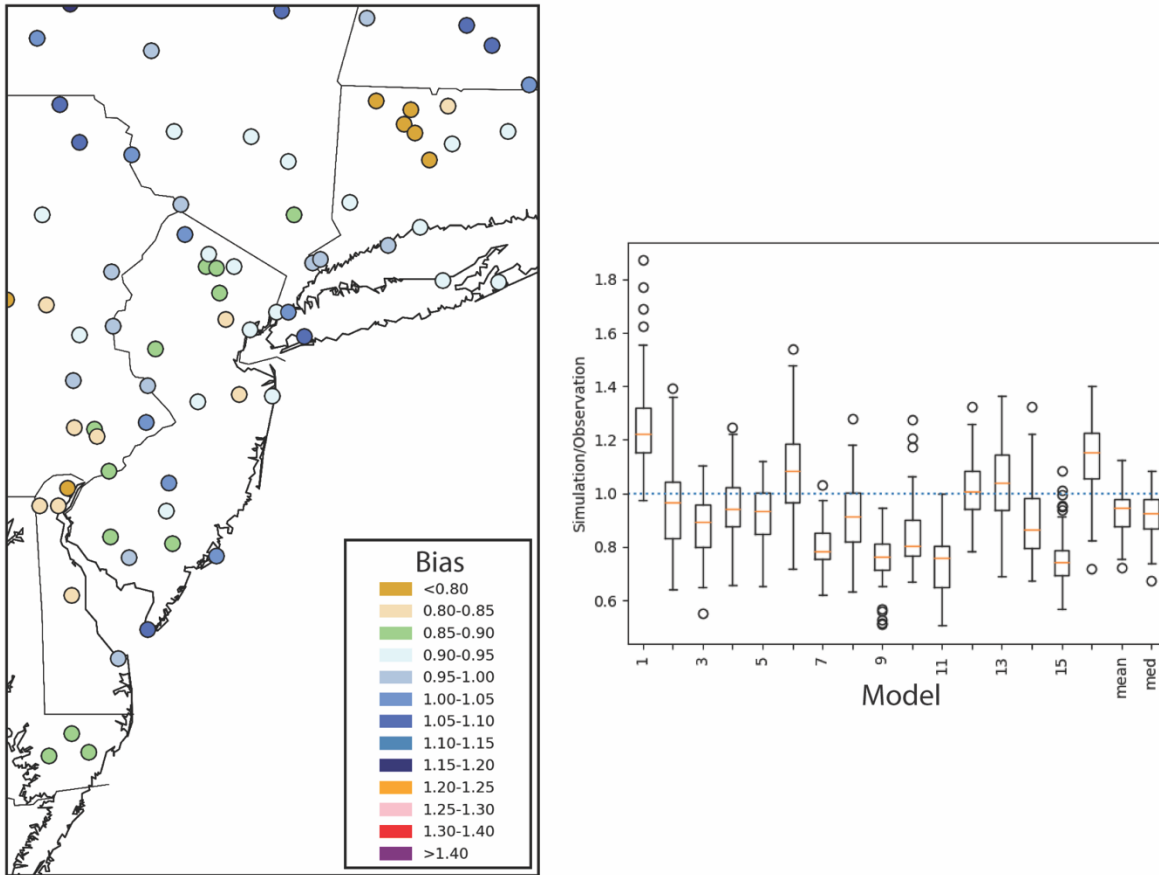*Figure 7. As in Figure 6 but for 10-yr ARI precipitation.*

Figure 8. As in Figure 6 but for 100-yr ARI precipitation.

c. CORDEX RCP 4.5

The set of available CORDEX models was different under the RCP 4.5 scenarios, with the base resolution of some of the simulations coarser than those for RCP 8.5. Therefore, unlike LOCA, for which the same models and spatial resolutions exist for the RCP8.5 and RCP4.5 scenarios, the historical biases needed to be assessed separately for this independent set of CORDEX models.

In general, the RCP4.5 CORDEX model bias is similar to that for the RCP8.5 models. Individual models both over and underestimate the observed ARI precipitation amounts, with the

degree of underestimation increasing as the ARI lengthens (Figures 9-11). For the 100-yr ARI, all but two models underestimate the observed values, with the median bias of the CanESM-RCA4 and EC-EARTH-RCA4 combinations indicating only 60% of the observed value (Fig, 11). These are the only combinations that use the RCA4 regional model. Underestimates of this magnitude are the largest of any of the downscaled data sets. Across the models, median biases range from 70-120% for the 2-yr ARI and 65-120% for the 100-yr ARI. These ranges of model-specific median bias are larger than those for the RCP8.5 CORDEX models. Like the other downscaled datasets, coastal stations are associated with the largest underestimates and the bias at more inland locales transitions to either a smaller degree of underestimation or in some cases overestimation of the observed values.
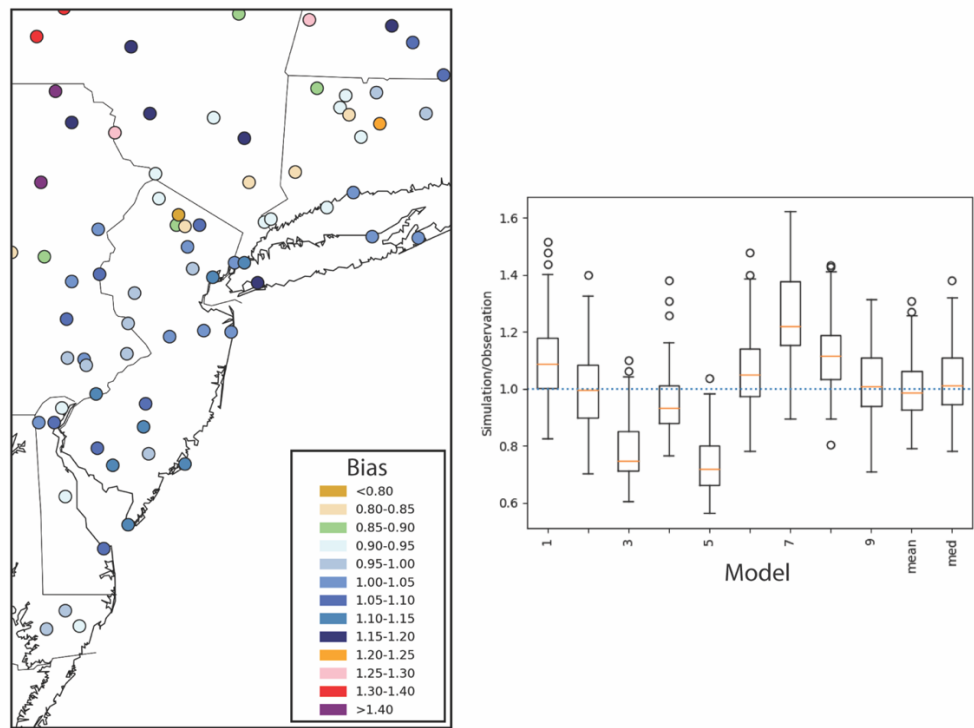
Figure 9. Bias associated with CORDEX RCP4.5 model simulations of 2-yr ARI precipitation

for the 1950-1999 historical period. In the map, the 9-model CORDEX median is

shown for each station. The boxplots show the bias for each model (numbers
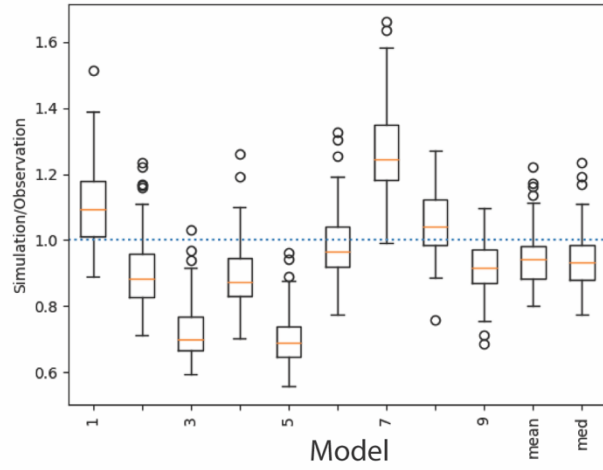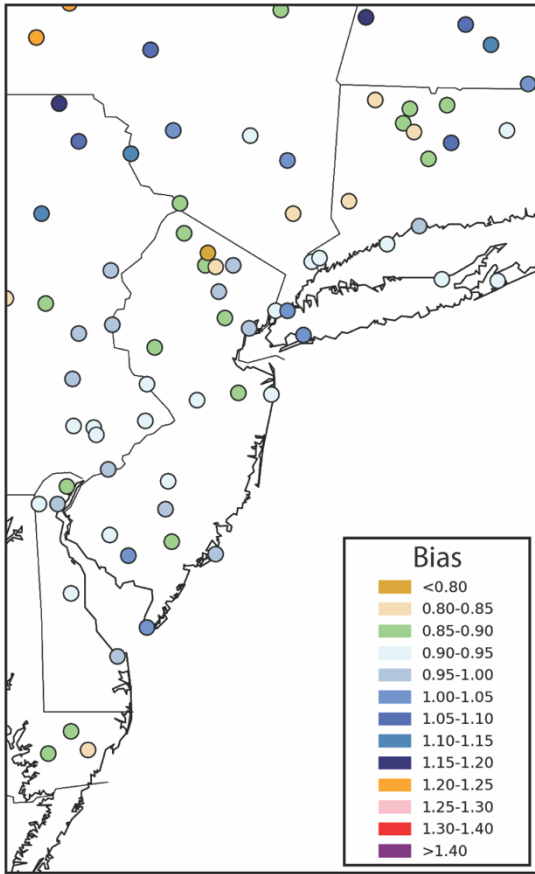
correspond to models listed in Table 3) across all stations.

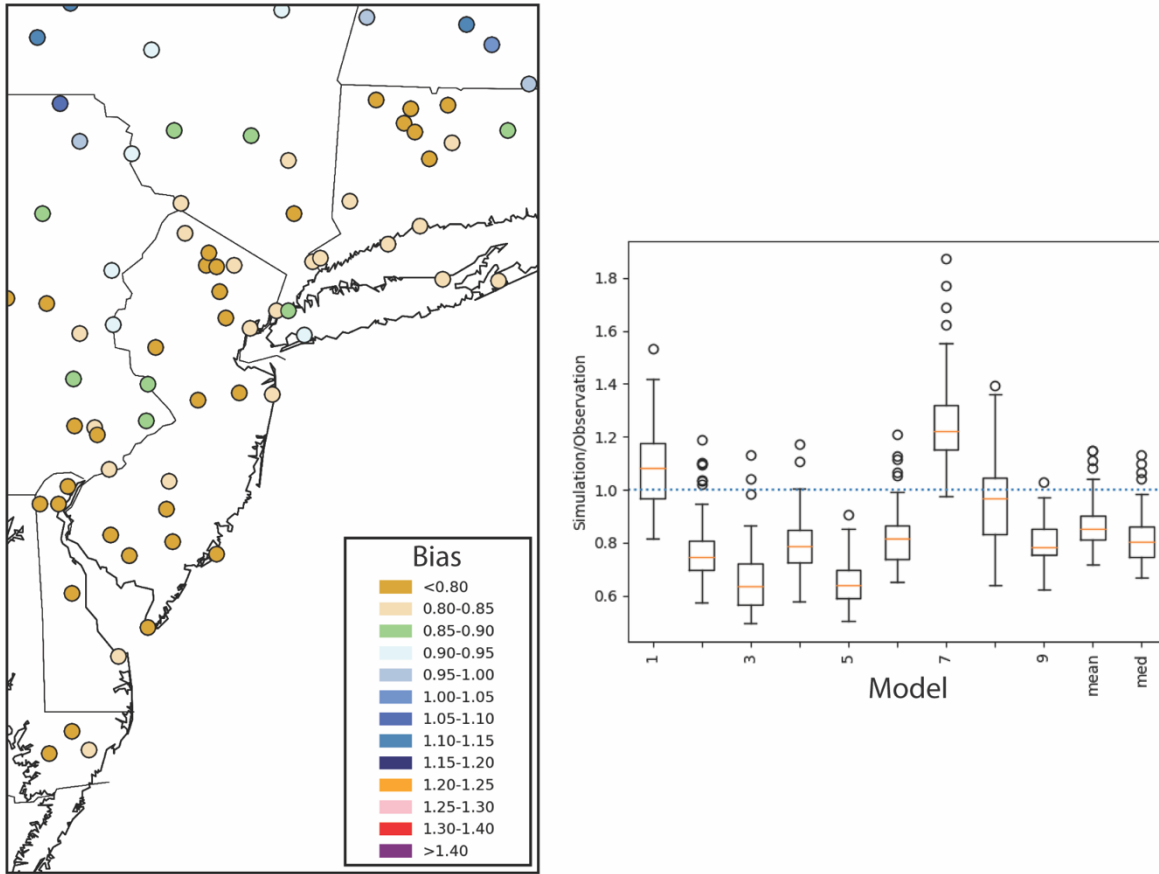*Figure 10. As in Figure 9 but for 10-yr ARI precipitation.*

Figure 11. As in Figure 9 but for 100-yr ARI precipitation.

ii. Model-Specific RCP8.5 Projected Change (2050-2099)

Biases such as those described in the proceeding section are not uncommon in downscaled

climate model data. To account for these biases, future changes are typically expressed as a

difference between the model values projected to occur in some future period and those

simulated in the historical period. In this approach, the bias is assumed to be constant throughout

the modeling period (i.e. the same bias exists in the future and historical model periods) and

therefore the resulting difference can be ascribed to the change in climate. Applying these

differences to observed data from the same period as the models' historical simulation,

effectively serves as a means of bias-adjusting the model simulation as the bias-free model

difference is applied to the observations. In this section, the model-specific change factors in the 2050-2099 period are discussed to elucidate uncertainty inherent to the different models and downscaling techniques. Similar features characterize the 2020-2069 period and thus are not shown for the individual models. Summary results for this early period are provided in the next section.

a. LOCA RCP8.5 2050-2099

For the LOCA-downscaled models, 2-yr and 10-yr ARI precipitation increases by 10-20% across the state in the 2050-2099 period under RCP 8.5 (Figs. 12 and13). There is considerable model-to-model consistency in this change, with 75% of the model medians falling between 15 and 20% (Fig. 12 and 13). At a small subset of stations, all models indicate a decrease in 2-yr ARI rainfall, with a single model (inmcm4) indicating a decrease at nearly half the stations (Fig. 12 and 13). The smallest LOCA-model median increases (5-7.5%) are concentrated in central NJ along the Delaware River (Figs. 12 and 13). Increases of between 15 and 20% are common in southern New Jersey. The largest increases occur in the extreme northern part of the state with increases in the 20-25% range for 2-yr ARI and the 25-30% range for 10-yr ARI.

For 100-yr ARI rainfall, the variation between models is greater, most show a median increase of between 10 and 30%, but two in two models (CESM1-CAM5 and GFDL-CM3) a decrease in 100-yr ARI precipitation is indicated at the majority of stations (Fig. 14). Conversely, median increases in excess of 30% are given by several models. Many models show a doubling of 100-yr ARI precipitation at some stations with the BNU-ESM model data projecting rainfall to more than triple at several stations (Fig. 14). The spatial pattern of CFs is very pronounced for the 100-yr ARI precipitation. The smallest changes (slight decreases to 5% increases) are concentrated in and around New York City, with increases in the 5-10% along the

NJ coast and central parts of the state (Fig. 14). In extreme northern NJ and continuing into parts of Pennsylvania, New York and Connecticut, 100-yr ARI CFs exceed 1.40. The area of smaller increases in near New York City was not indicated in early work for the state of New York. However, a direct comparison of these two sets of results is not possible given differences in the downscaling techniques, GCMs, periods of record, and spatial resolutions used. In the New York work, some ensemble members did indicate decreases in 100-yr ARI in the vicinity of New York City in the 2070-2099 period the was evaluated.
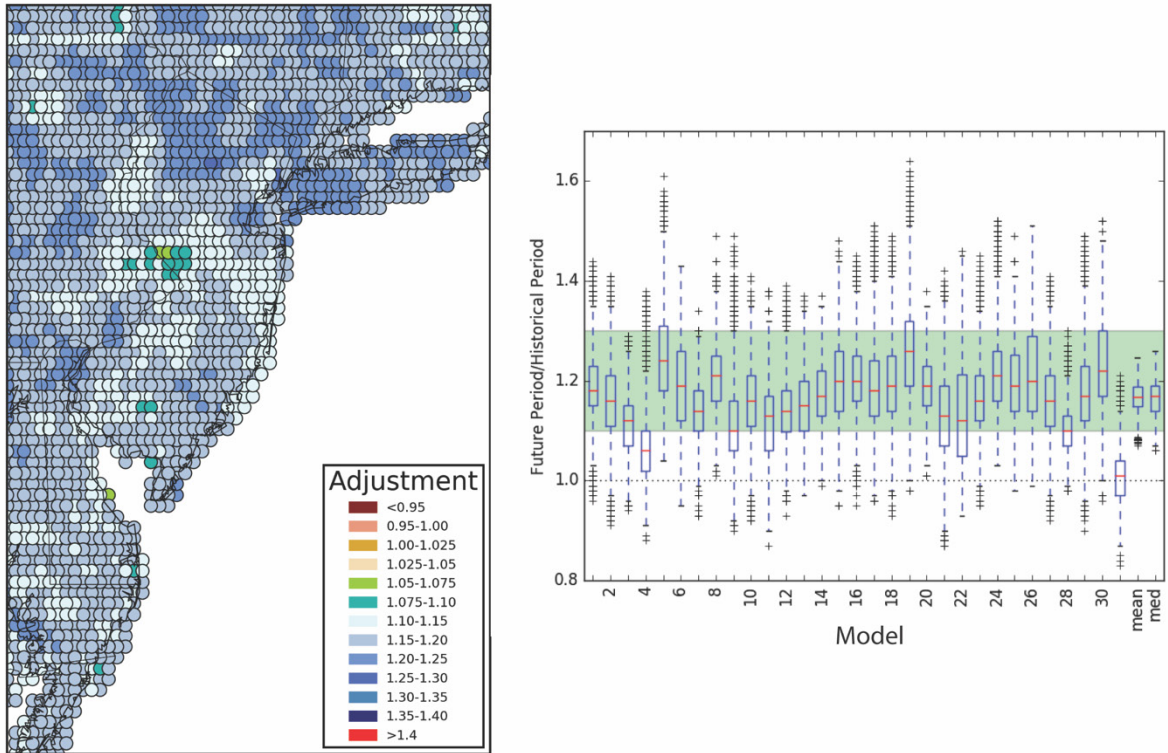

Figure 12. Change in 2-yr ARI precipitation in 2050-2099 under RCP 8.5 relative to the 1950-1999 historical period. In the map, the 31-model LOCA model median is shown for each LOCA grid point. The boxplots show the change for each model (numbers correspond to models listed in Table 2) across all grid points.
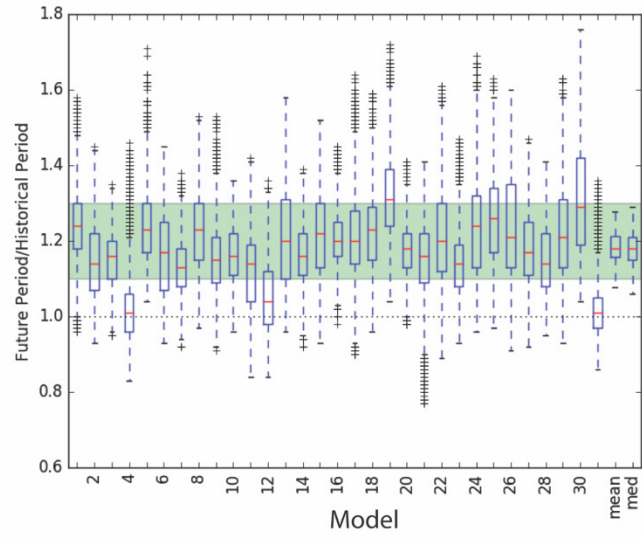
Figure 13. As in Figure 12 but for 10-yr ARI precipitation

Figure 14. As in Figure 12 but for 100-yr ARI precipitation

b. LOCA RCP4.5 2050-2099

For the lower RCP4.5 emissions scenario, the magnitude of future change is less as expected. For 2-yr ARI precipitation, the model-median change is near 10% (Fig. 15). Individual models show median changes of between 3 (inmcm4) and 17% (CMCC-CM). Similar changes are indicated for 10-yr ARI precipitation, however in most models the median increase is higher, with IPSL-CM5A-MR simulating a >20% increase (Fig. 16). The spatial pattern of model-median change is similar to that under RCP8.5. Smaller (5-10% increases are typical in the center of the state and the largest increases (15-20%) located in the north. This pattern is exaggerated when the 100-yr ARI is considered. Grids in the vicinity of New York City and in central NJ show small (<5%) decreases in 100-ARI rainfall (Fig. 17). In northern parts of the

state increases in the 25-35% range are common. In two models (CMCC-CMS) and (GFDL-CM3) decreases in 100-yr ARI precipitation are indicated at more than half of the grid points in the domain, while in several models 100-yr ARI precipitation increases at nearly all grids.

Figure 15. Change in 2-yr ARI precipitation in 2050-2099 under RCP 4.5 relative to the 1950-1999 historical period. In the map, the 31-model LOCA model median is shown for each LOCA grid point. The boxplots show the change for each model (numbers correspond to models listed in Table 3) across all grid points.
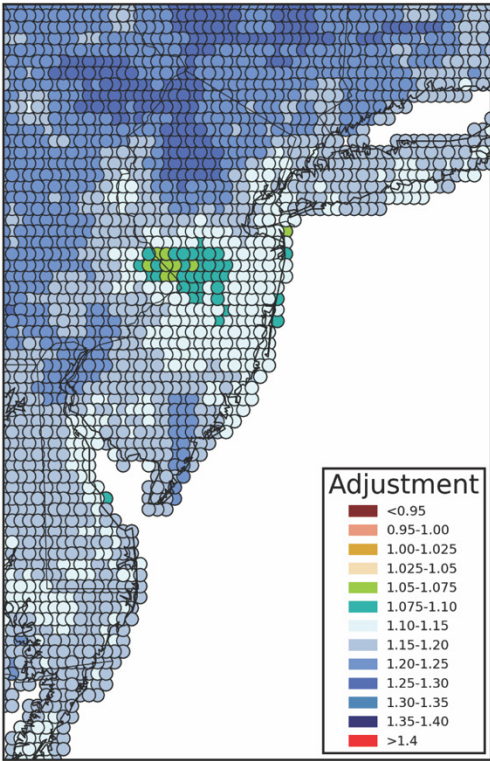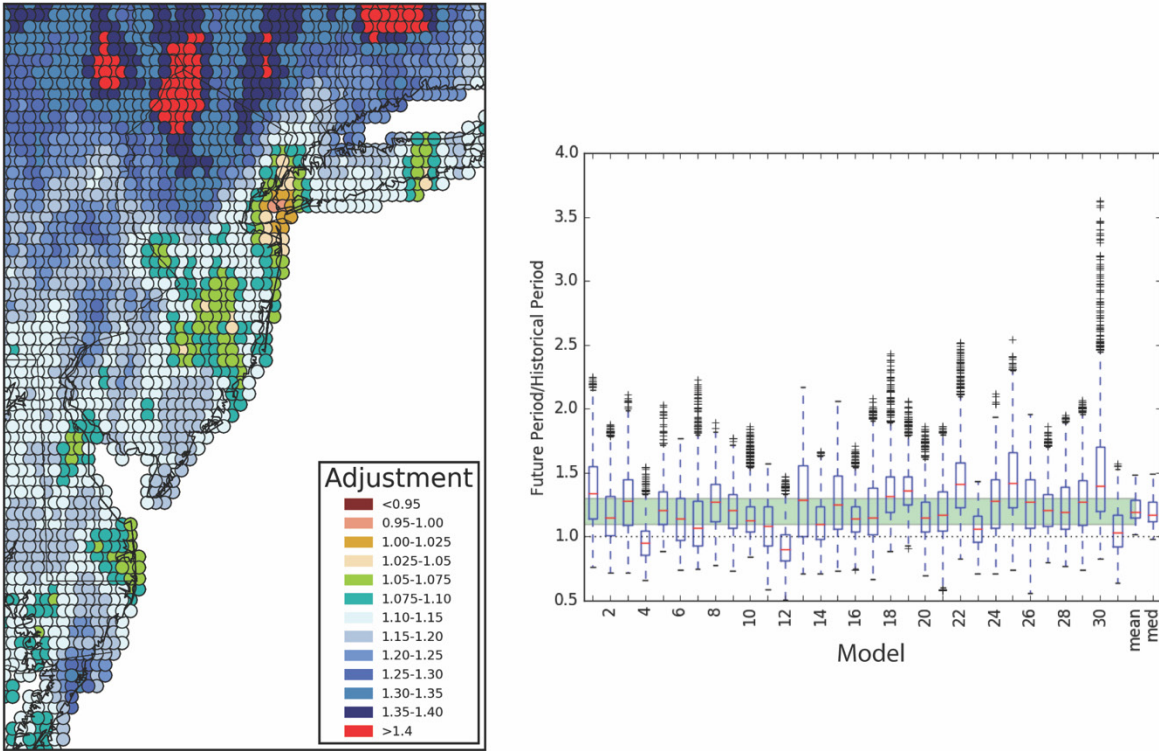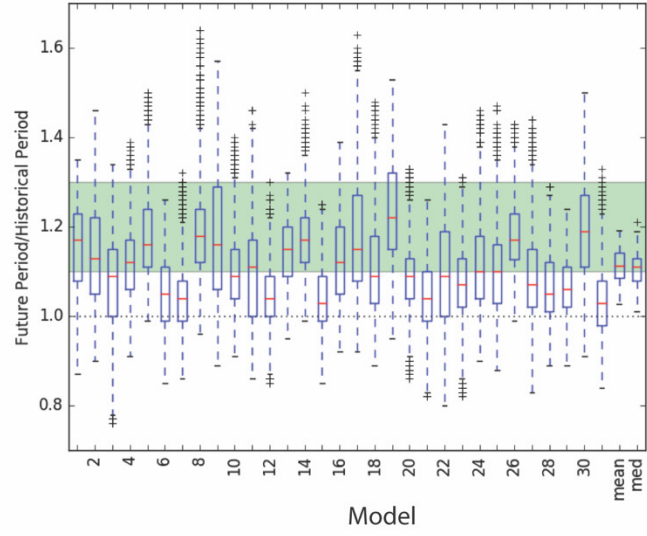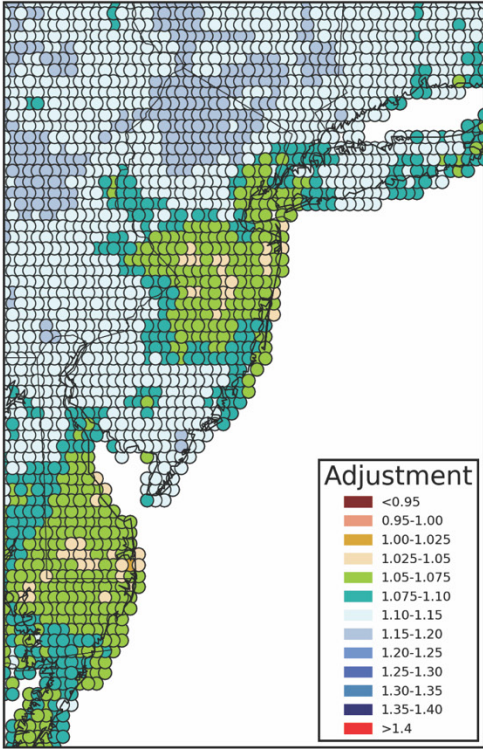
Figure 16. As in Figure 15 but for 10-yr ARI precipitation

Figure 17. As in Figure 15 but for 100-yr ARI precipitation

c.   CORDEX *RCP8.5 2050-2099*

The CORDEX model projections of 2-, 10- and 100-yr ARI rainfall under RCP8.5 for the

2050-2099 period were characterized by similar, although slightly smaller median increases than

those given by the LOCA models. For both the 2-yr and 10-yr ARIs, median increases are in the

10-20% range at most grid points (Figs. 21-22). The smallest median increases were associated

with the MPI-ESM-MR-CRCM5_UQAM model combination, while the CanESM2-CRCM4

model combination indicated increases in excess of 20% at the majority of grid points. In most

model combinations decreases were limited to just a few stations.

For the 100-yr ARI, the median increases were slightly higher with the grid point median

increase exceeding 20% for several models (Fig. 23). This is similar to the LOCA models in

which the median 100-yr ARI CF for some increased from those associated with 2-yr and 10-yr

ARI.   Although the coarse resolution of the CORDEX simulations prevents a detailed analysis

of the spatial pattern of changes, the general pattern runs counter to that for LOCA. Especially

for the 100-yr ARI, the smallest CFs are located inland in the northwest corner of the study
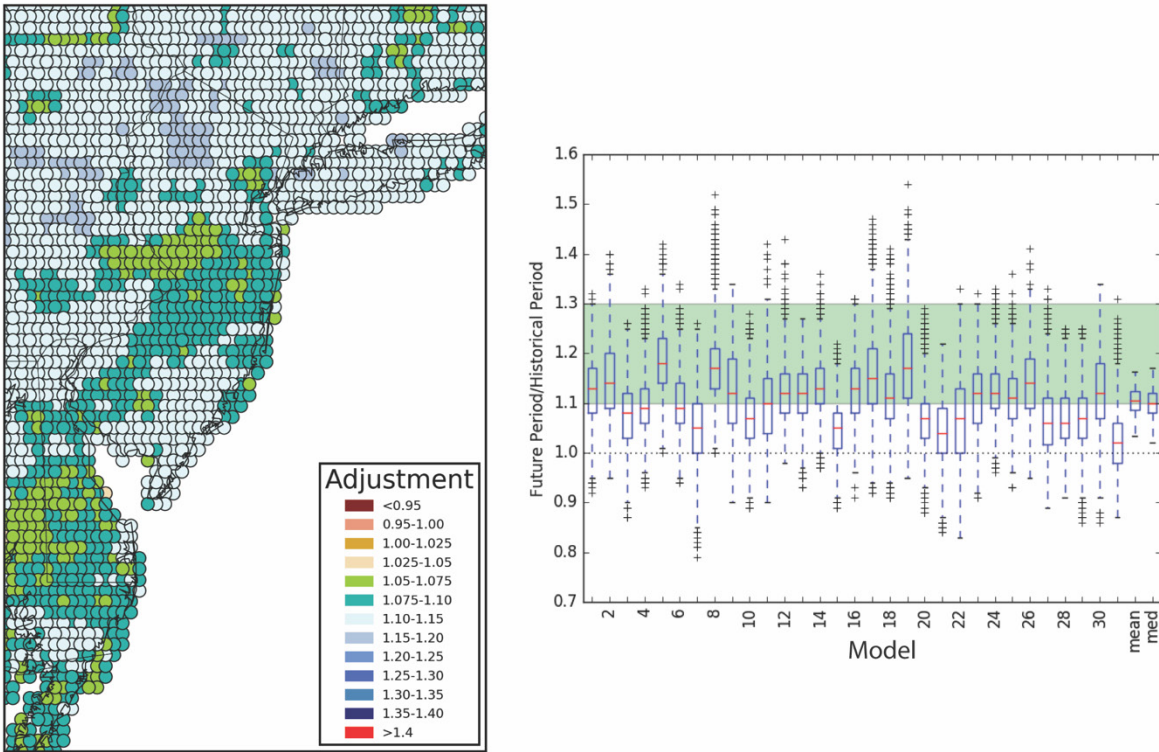
domain (Fig. 23).

Figure 21. Change in 2-yr ARI precipitation in 2050-2099 under RCP 8.5 relative to the 1950-
1999 historical period. In the map, the 16-model CORDEX model median is shown
for each CORDEX grid point. The boxplots show the change for each model
*(numbers correspond to models listed in Table 3) across all grid points.*

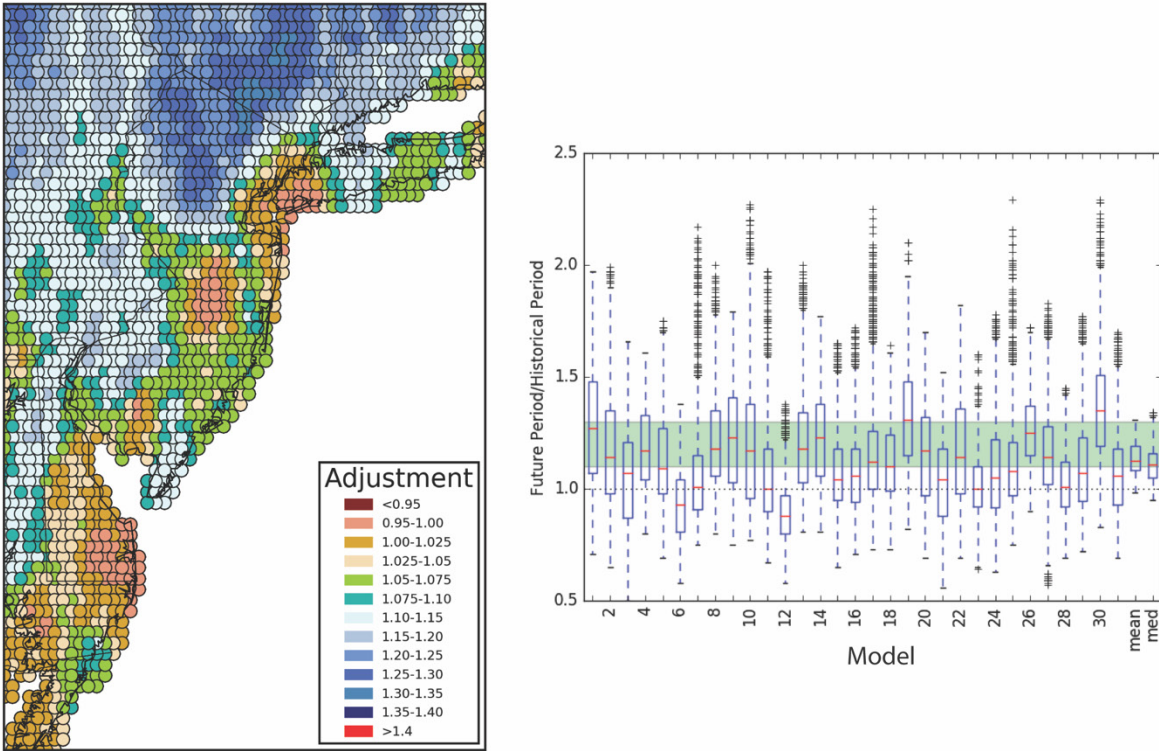*Figure 22. As in Figure 21 but for 10-yr ARI precipitation*

Figure 23. As in Figure 21 but for 100-yr ARI precipitation

d. CORDEX *RCP4.5 2050-2099*

Under RCP4.5, the CORDEX model projections of 2-, 10- and 100-yr ARI rainfall for the 2050-2099 period were characterized by consistently larger median increases that those given by the LOCA models. For both the 2-yr and 10-yr ARIs, median increases are in the 10-15% range at most grid points (Figs. 24-25), whereas particularly in the center of the state the LOCA projections fell in the 5-10% range. The smallest median increases were associated with the GEMatm-Can-CRCM5-UQAM, GFDL-ESM2M-RegCM4 and GFDL-ESM2M-WRF model combinations, while the GFDL-ESM3M-CRCM5-OUR model combination indicated increases in excess of 20% at the majority of grid points. Across the models, decreases were limited to just a few stations.

For the 100-yr ARI, the median increases were slightly lower with the grid point median increase falling below 10% for more models (Fig. 26). This is similar to the LOCA models in which the 100-yr ARI CF for some gridpoints decreased from those associated with 2-yr and 10-yr ARI. Although the coarse resolution of the CORDEX simulations prevents a detailed analysis of the spatial pattern of changes, there is a tendency for smaller increases in the central and southern parts of the study domain, especially for the 100-yr ARI. This is similar to the LOCA pattern of larger increases to the north and smaller increases in the south.
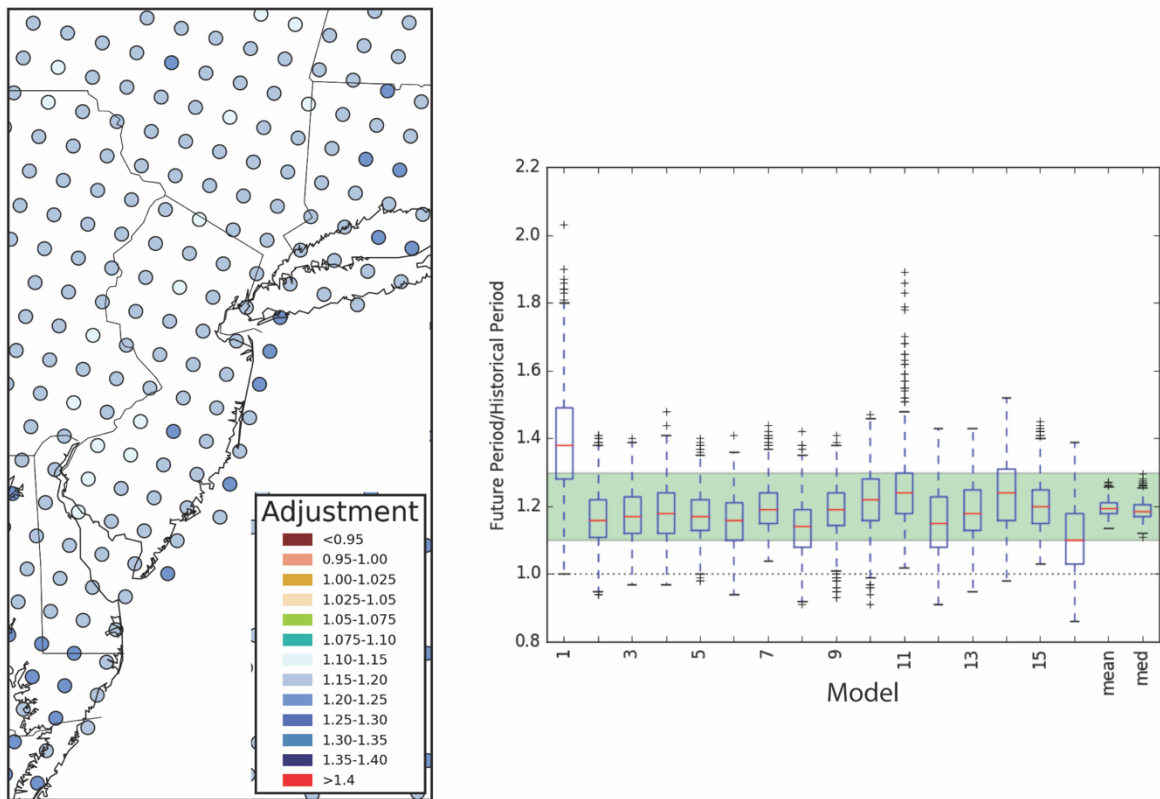

Figure 24. Change in 2-yr ARI precipitation in 2050-2099 under RCP 4.5 relative to the 1950-1999 historical period. In the map, the 9-model CORDEX model median is shown for each CORDEX grid point. The boxplots show the change for each model (numbers correspond to models listed in Table 3) across all grid points.
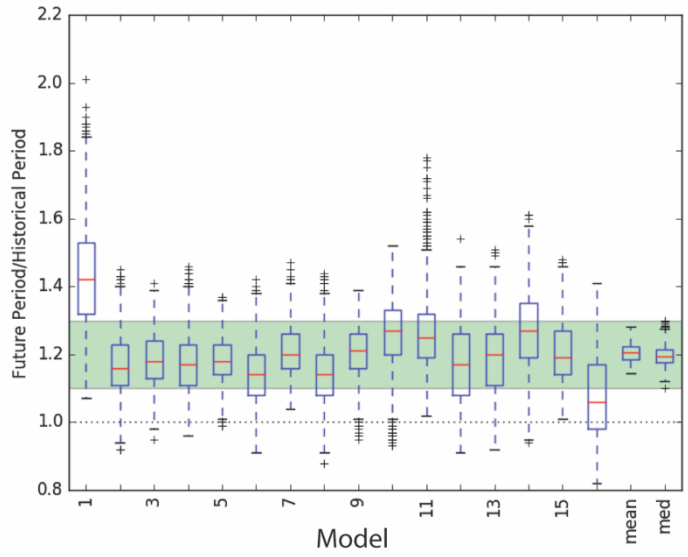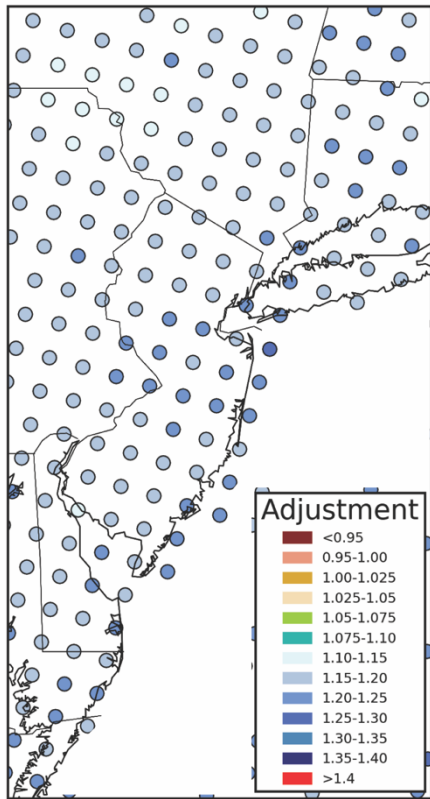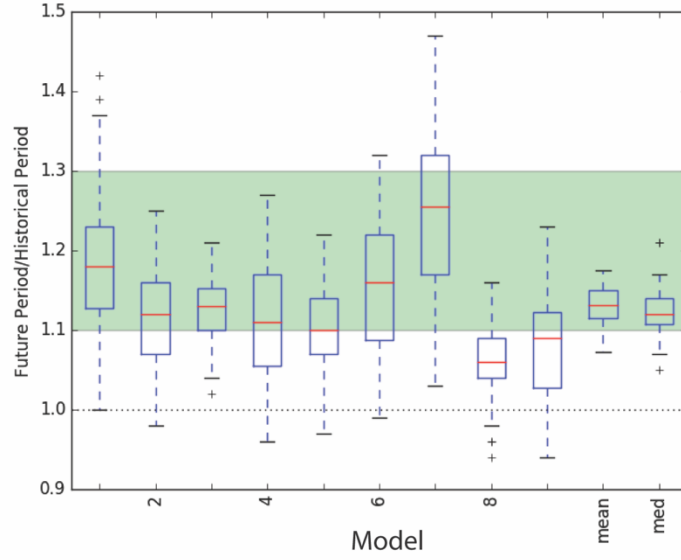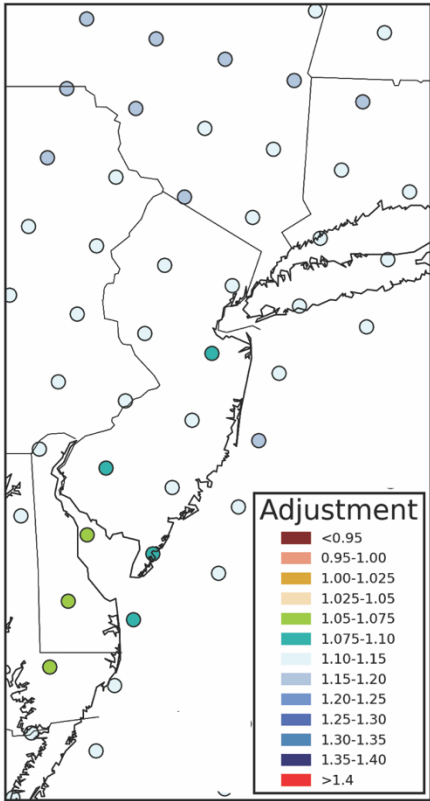
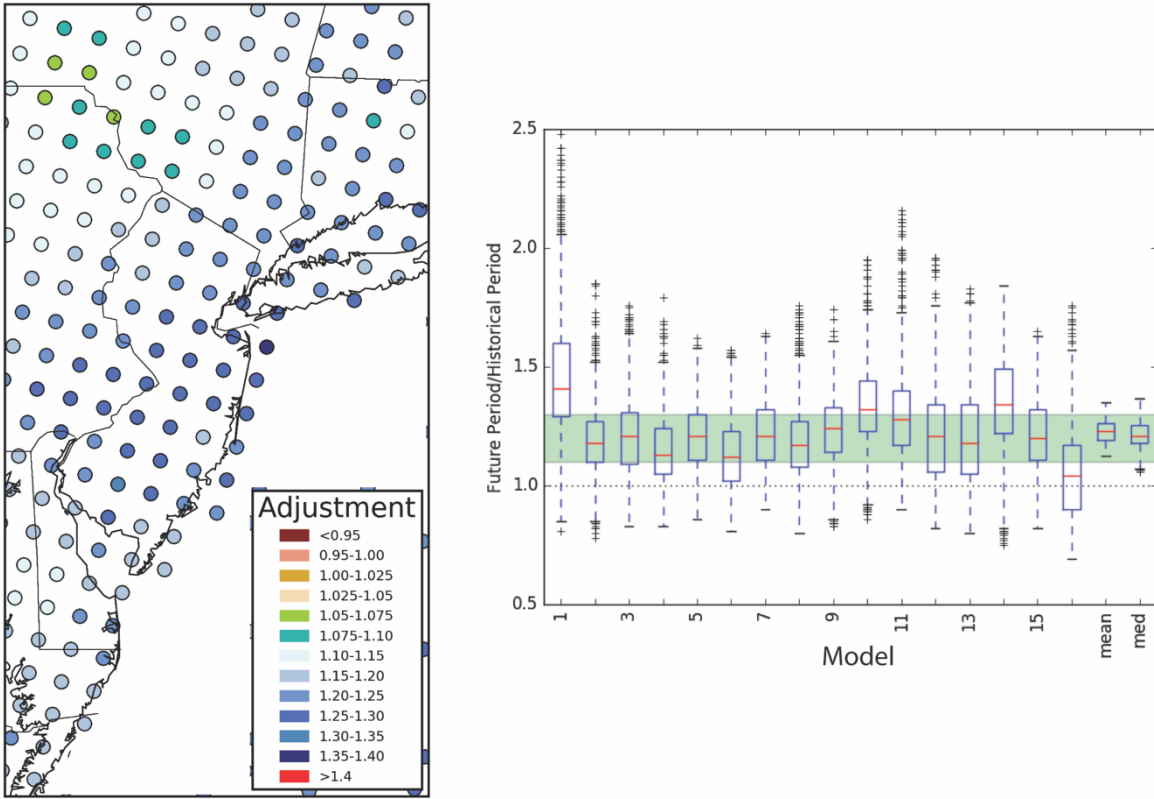*Figure 25. As in Figure 24 but for 10-yr ARI precipitation*
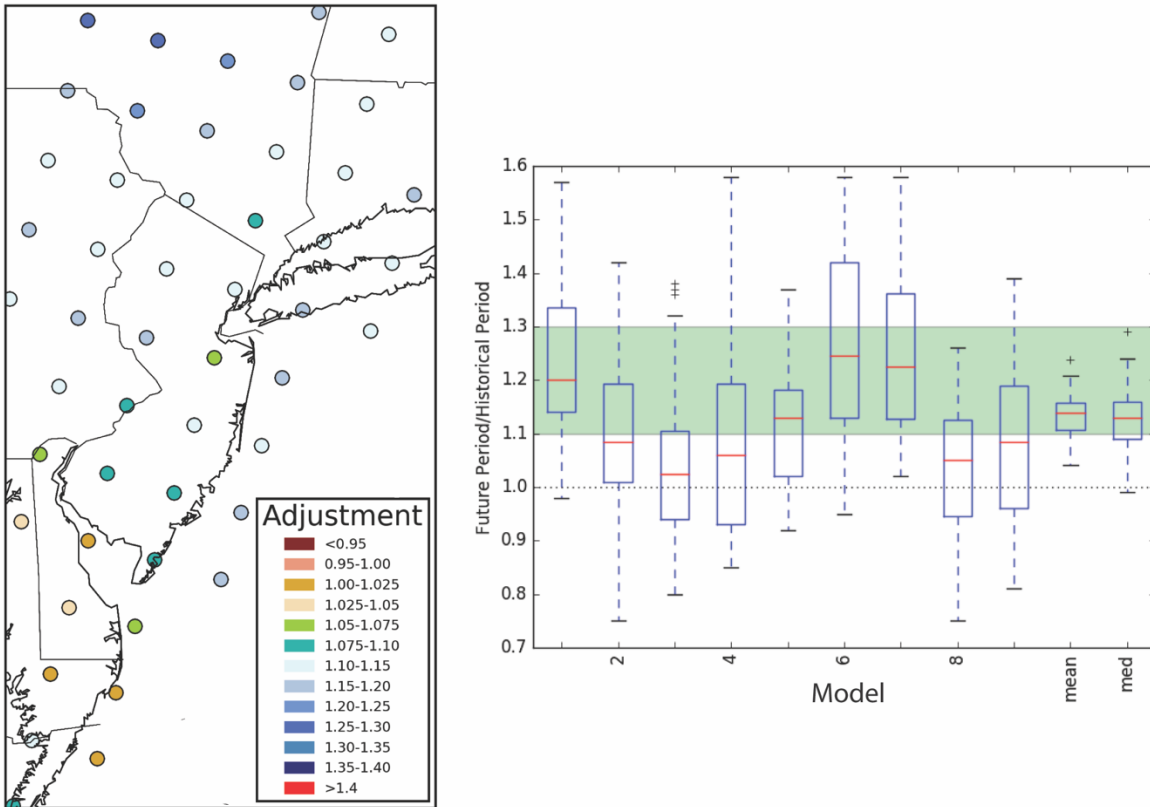
Figure 26. As in Figure 24 but for 100-yr ARI precipitation

iii. Ensemble change factors

The CFs from the individual models were combined to give a single set of change factors. Here the LOCA and CORDEX results were interpolated to a common 0.1° grid and from the resulting set of 47,000 (47 models x 1000 simulations) change factors the median, 17th and 83rd percentiles extracted. Approximately two thirds of these simulations fall between the 17th and 83rd percentiles. The 25th, 75th, 10th and 90th percentiles were also extracted. Each of the figures below consist of three panels showing the 17th and 83rd percentile confidence bounds as well as the ensemble median change factors.

a. 2050-2099 RCP8.5

For the 2 yr ARI (Fig. 27), the median change factors under the high emissions scenario, were consistently in the 1.15-1.20 range across the state, with the exception of an area of 1.10-1.15 values on across the central part of the state. The lower bound of the 17th-83rd percentile uncertainty range was generally in the range of 1.05 to 1.10, with lower values in central NJ and higher values to the north. At the upper end of the uncertainty range, most CFs are in the 1.25-1.30 range with higher (1.30-1.35) values in the north and a few areas of lower (1.20-1.25) CF values along the coast and across the middle of the state.

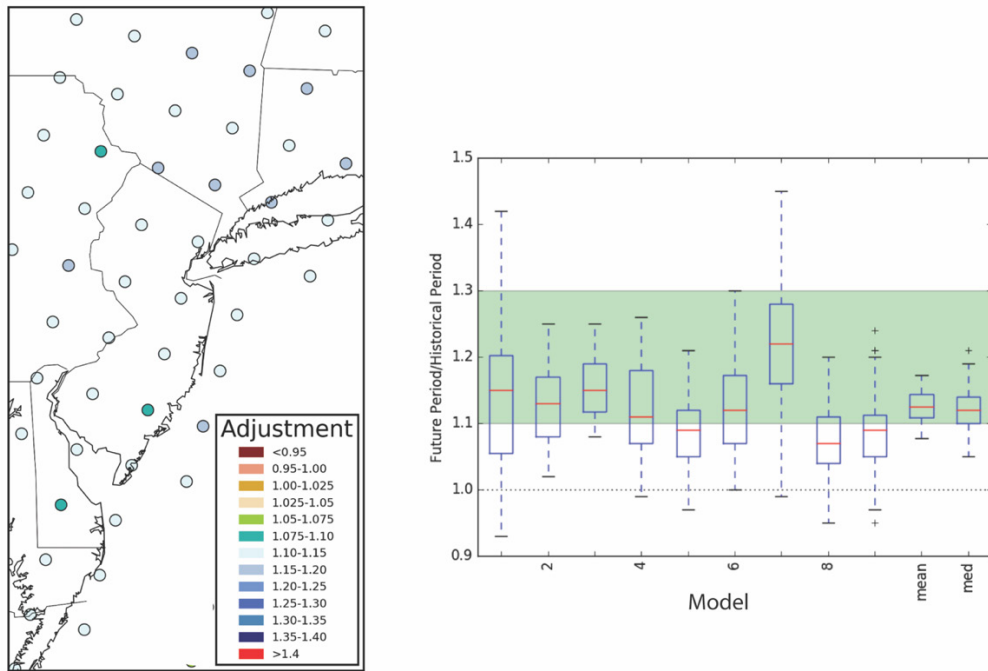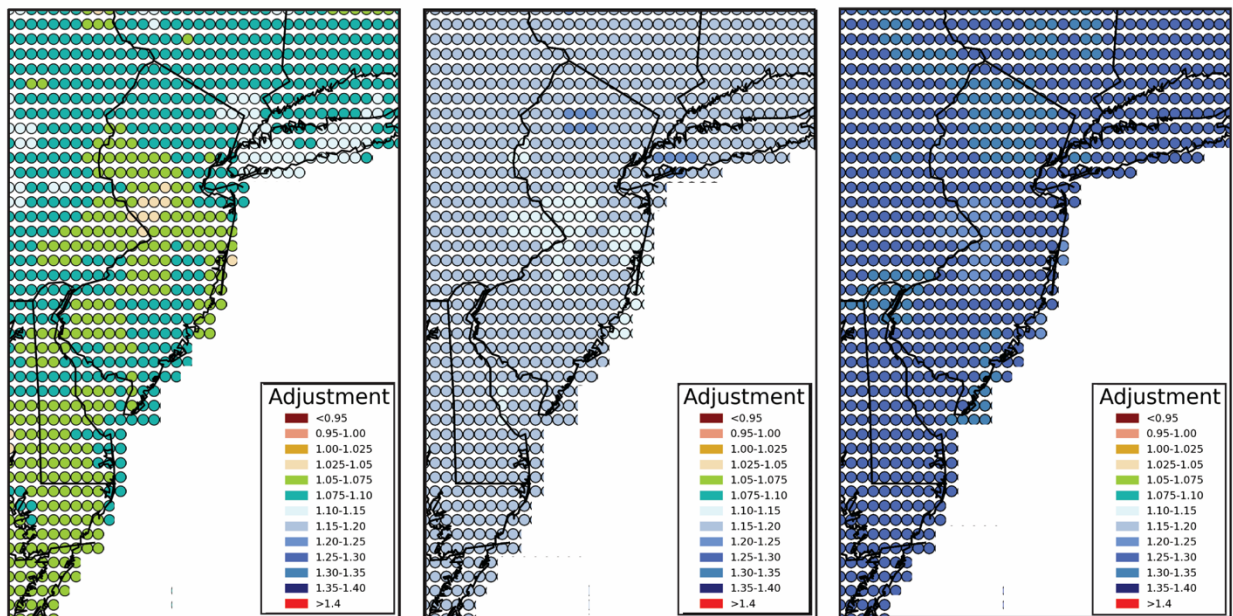*Figure 27. Change in 2-yr ARI precipitation in 2050-2099 under RCP 8.5 relative to the 1950-1999 historical period for the ensemble of LOCA and CORDEX downscaled models. The lefthand panel shows the 17th percentile of the ensemble at each 0.1° gridpoint. The ensemble median is given in the center panel and the 83rd percentile of the ensemble shown in the rightmost panel.*

The 10-yr ARI median change factors are similar to the 2-yr values, generally ranging from 1.15 to 1.20, but with higher 1.20-1.25 values to both the north and along the southern coast and lower 1.10-1.15 CFs in the central part of the state (Fig. 28). The uncertainty bounds are also similar to the 2-yr values, except for an area smaller 1.025-1.05 values characterizing the lower end of the uncertainty range in central NJ and generally higher values defining the upper uncertainty bound especially in northern NJ were many grids fall into the 1.35-1.40 range.
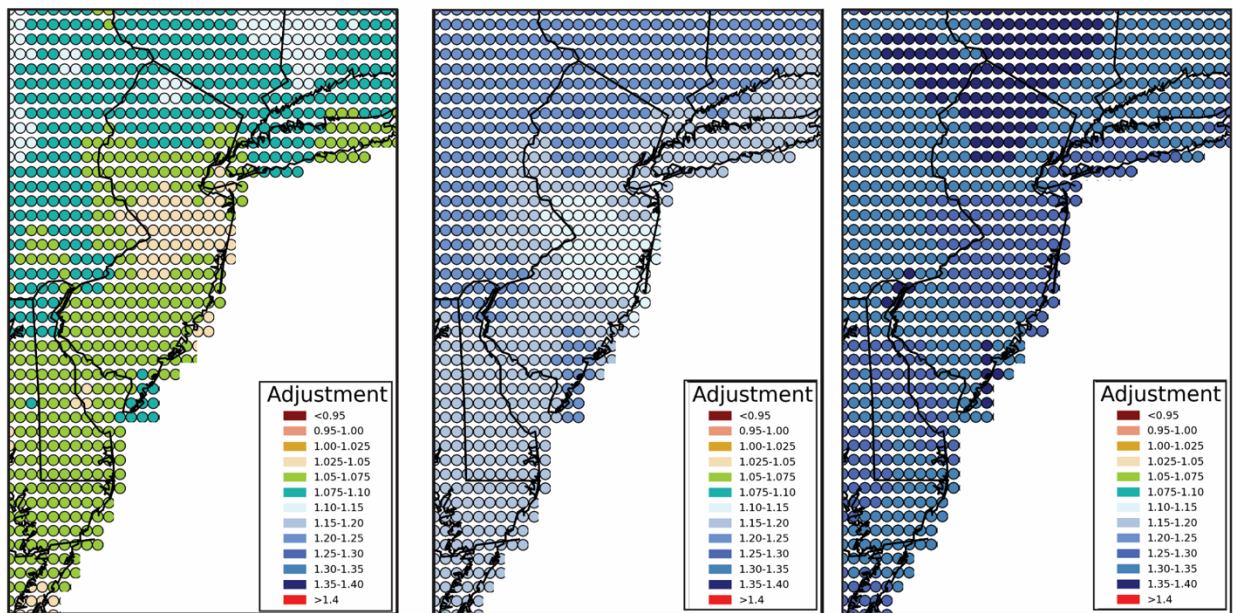
Figure 28. As in Figure 27 but for the 10-year ARI.

The range of median 100-yr CFs expands relative to those for the shorter ARIs (Fig. 29). In the New York City area a few grid points have CF values as low as 1.075-1.10, while median CF values in extreme northern NJ fall into the 1.35-1.40 range. In the majority of the state, median CF values for the 100-yr ARI fall between 1.10 and 1.20. The uncertainty range for the 100-yr ARI CFs is quite large. At the lower end, the models project a decrease in 100-yr ARI

rainfall across the majority of the state (Fig. 29), with CF values mainly in the 0.95 -1.00 range, but in some locations the 17th percentile CF values fall below 0.95. At the upper end of the uncertainty bound, a large part of northern NJ has 83rd percentile CF values in the 1.50-1.60 range with some grids exceeding 1.70. In coastal areas the upper uncertainty bound is only in the 1.20-1.25 range.
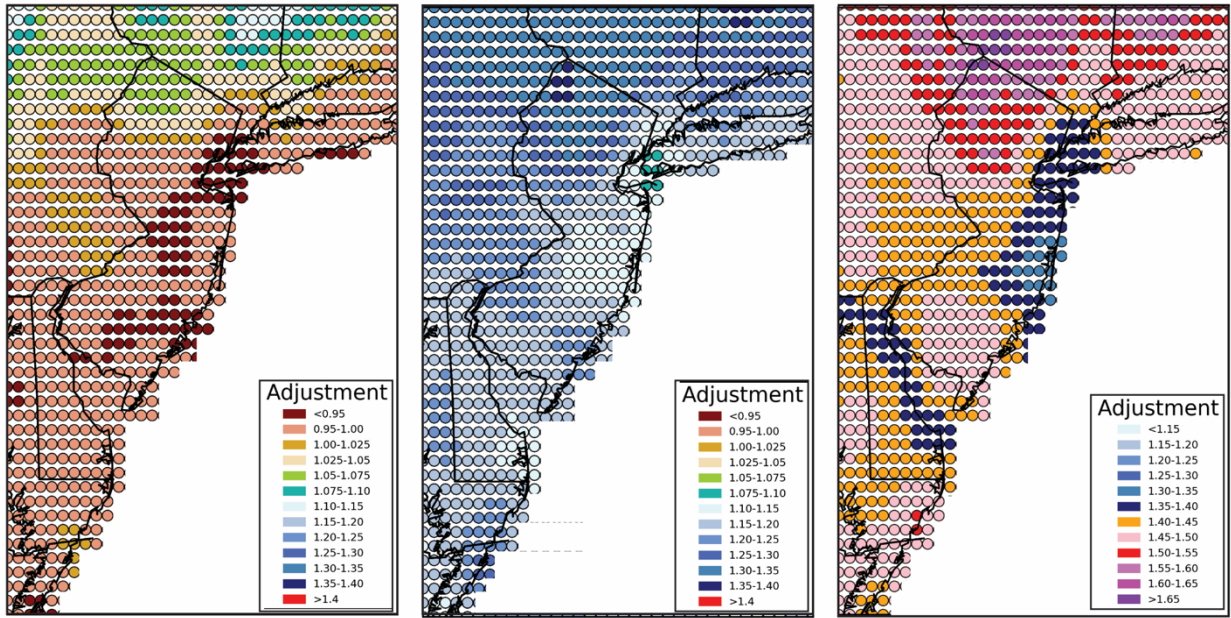
Figure 29. As in Figure 27 but for the 100-yr ARI

b. 2050-2099 RCP 4.5

Under the more moderate RCP4.5 emissions scenario, the CFs during the 2050-2099 period decrease. The median 2-yr ARI values range from 1.075-1.15 with the lower values again across the middle of the state (Fig. 30). Median 10-yr ARI change factors range from 1.05 to 1.15 with the highest values in northern NJ and the lowest (1.05-1.075) values covering a large area from New York City, along the NJ coast and across a broad area of central NJ (Fig. 31). The median CFs associated with the 100-year ARI, range from as low as 1.00-1.025 near New

York City to as high as 1.20-1.25s near High Point (Fig. 32). In the majority of central and southern NJ CFs are in the 1.075-1.15 range.

The lower uncertainty bound for 2-yr ARI under RCP4.5 is close to 1.00 (1.00-1.025) across most of the state, with higher (1.05-1.075) values in the north and a few grid points associated with values <1.00 in central NJ (Fig 30). The lower bound for the 10-yr ARI is consistently in the 0.95-1.025 range across the state with values greater 1.05 confined to the northwest corner (Fig. 31). For the lower bound of the 100-yr ARI CFs, a larger area of the states associated with < 0.95 CFs (Fig. 32). The upper uncertainty bounds for both the 2-yr and 10-yr ARI are typically between 1.15 and 1.25 (Fig. 30 and 31). CFs in the 1.25-1.30 range characterize the upper bound of the 10-yr ARI in northern NJ (Fig. 31) and cover the majority of the state for the 100-yr ARI (Fig. 32). In northern NJ, CFs near the upper bound of the uncertainty range exceed 1.50.
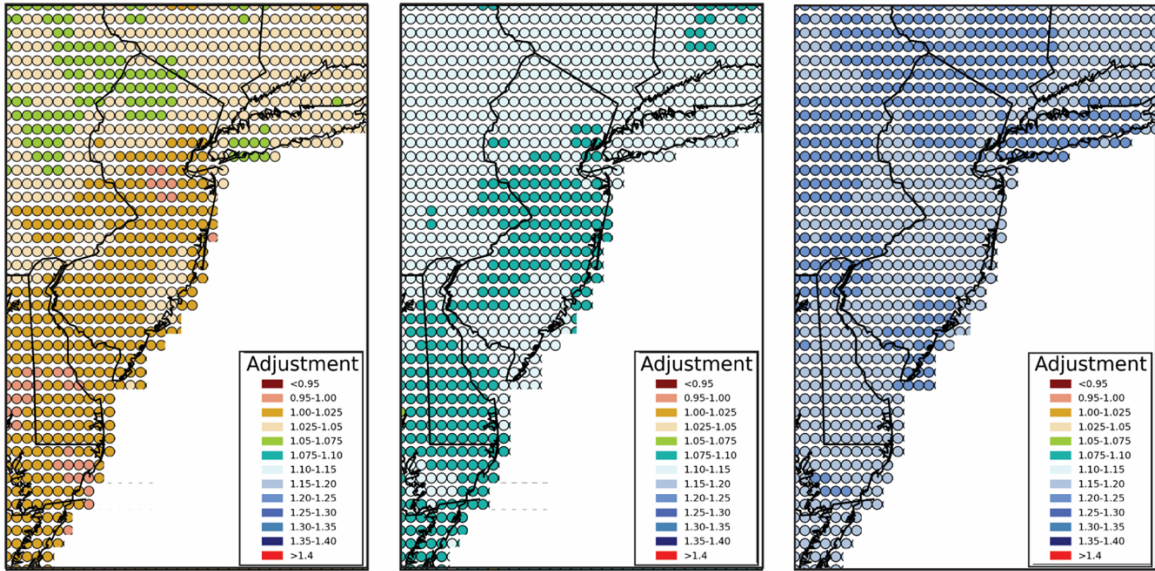
1999 historical period for the ensemble of LOCA and CORDEX downscaled models. The lefthand panel shows the 17th percentile of the ensemble at each 0.1° gridpoint. The ensemble median is given in the center panel and the 83rd percentile of the ensemble shown in the rightmost panel.
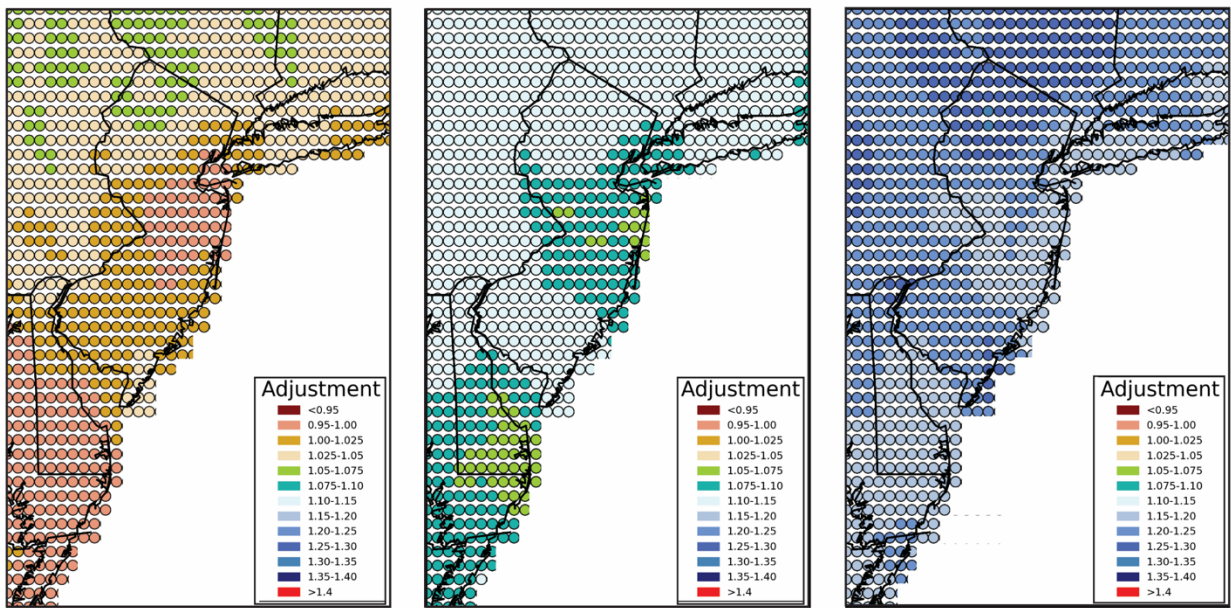
Figure 31. As in Figure 30 but for the 10-yr ARI.

Figure 32. As in Figure 30, but for the 100-yr ARI

c.   2020-2069 RCP 8.5

Mid-century (2020-2069) CFs under RCP 8.5 are similar to those for the end of the century under the more moderate RCP 4.5 emissions scenario, especially for the 2-yr and 10-yr ARI. The median 2-yr ARI values are generally in the 1.075-1.15 range with the same pattern of higher values north and lower values in the central part of the state (Fig. 33). Median 10-yr ARI change factors range from 1.05 to 1.15 with the highest values in northern NJ and the lowest (1.05-1.075) values in an area of central NJ (Fig. 34). The median CFs associated with the 100-year ARI, are in the 1.20-1.30 range in northern NJ, but only 1.05 or less in central New Jersey and along the coast near New York City (Fig 35).

In terms of the lower bound of the CF uncertainly range, decreases in 2-yr and 10-yr ARI are indicated by CF values in the 0.95-1.00 range (Fig 33 and 34) across much of the state, and decreases in 100-ARI precipitation are characterized by a large area of < 0.95 CFs (Fig. 35). The upper bounds of the 2020-2069 RCP8.5 confidence bounds are generally in the 1.15-1.20

range for the 2-yr ARI and 1.20-1.25 range for the 10-yr ARI (Fig 33 and 34). Like the other

cases there is considerable variation in the 100-yr ARI CFs with the upper bound of the

uncertainty range exceeding 1.50 in the north and the smallest values in the 1.15-1.20 range

along the coast (Fig. 35).
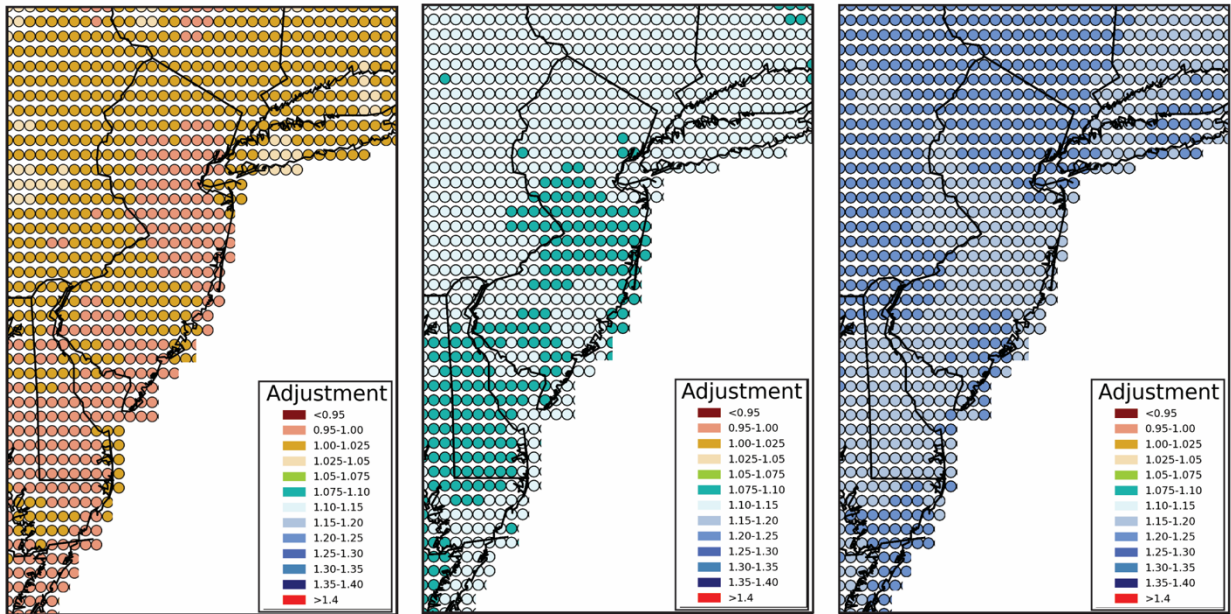
Figure 33. Change in 2-yr ARI precipitation in 2020-2069 under RCP 8.5 relative to the 1950-

1999 historical period for the ensemble of LOCA and CORDEX downscaled models.

The lefthand panel shows the 17th percentile of the ensemble at each 0.1° gridpoint.

The ensemble median is given in the center panel and the 83rd percentile of the

ensemble shown in the rightmost panel.
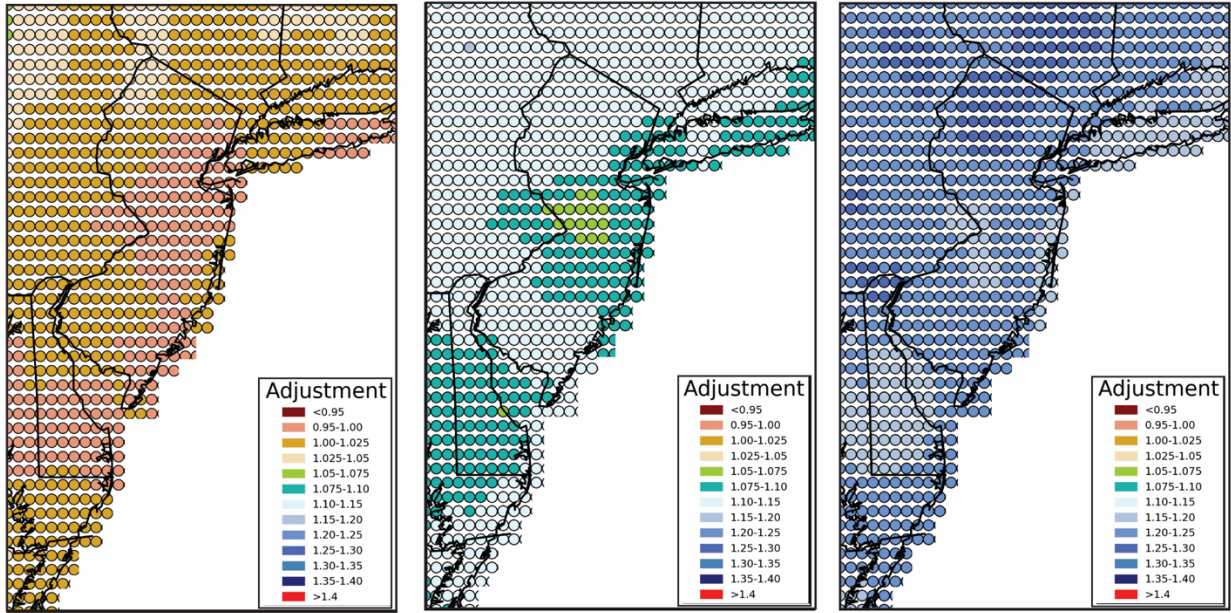
Figure 34. As in Figure 33, but for the 10-yr ARI
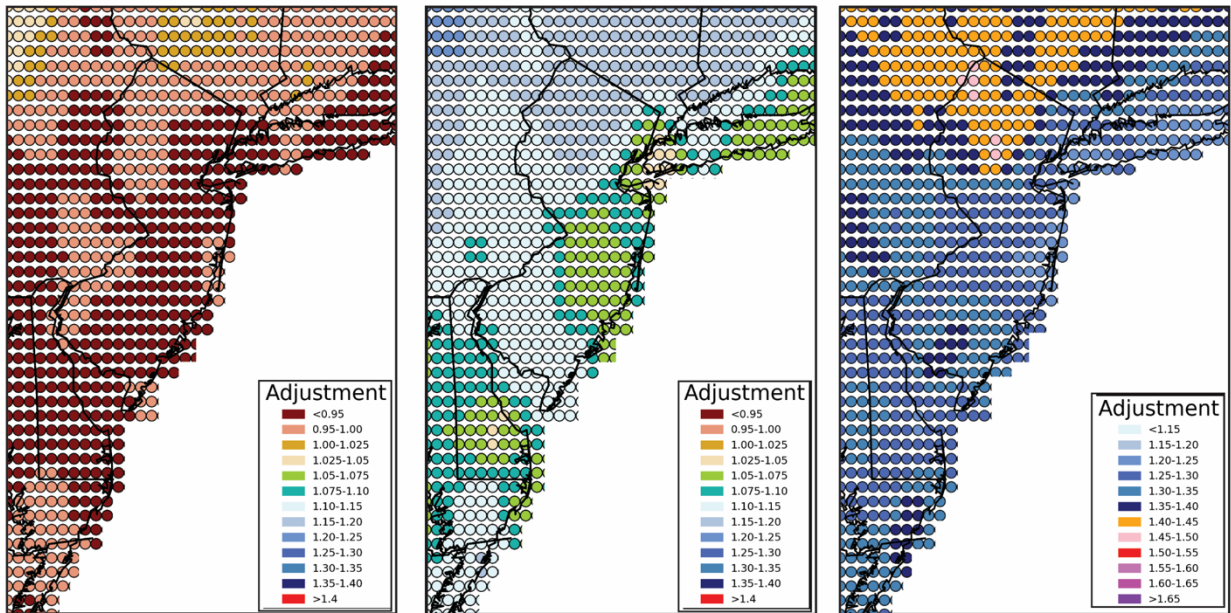
Figure 35. As in Figure 33, but for the 100-yr ARI.

d.   2020-2069 RCP 4.5

Finally, under the RCP4.5 emissions scenario, median CFs in the 1.05-1.10 range

characterize the 2-yr and 10-yr ARI (Fig. 36-37). While for the 100-yr ARI, lower 1.025-1.05

CFS occur in the vicinity of New York City and in central and coastal NJ and higher 1.10-1.15

cover the northern part of the state (Fig. 38). CF factors less than 1.00 again characterize the

lower uncertainty bound for the 2-, 10- and 100-yr ARI. The upper uncertainty bounds are

generally in the 1.15-1.20 range for the 2- and 10-yr ARI (Fig. 36-37) and exceed 1.25 in all but

coastal NJ for the 100-yr ARI. (Fig. 38).
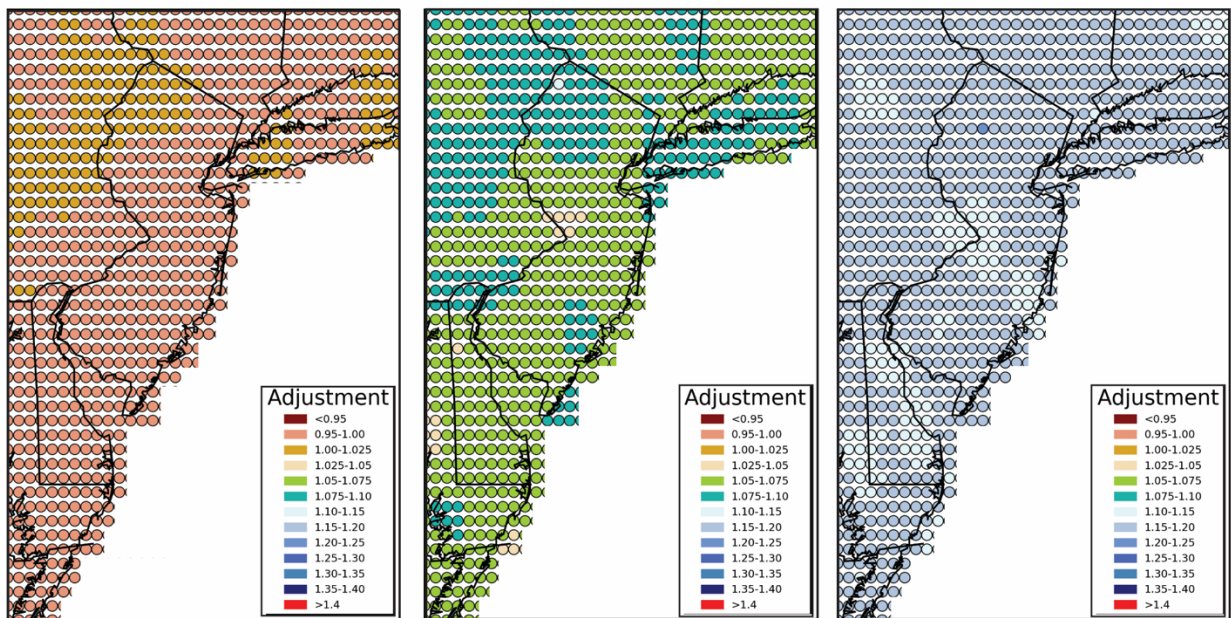
Figure 36. Change in 2-yr ARI precipitation in 2020-2069 under RCP 4.5 relative to the 1950-
1999 historical period for the ensemble of LOCA and CORDEX downscaled models.
The lefthand panel shows the 17th percentile of the ensemble at each 0.1° grid point.
The ensemble median is given in the center panel and the 83rd percentile of the
*ensemble shown in the rightmost panel.*

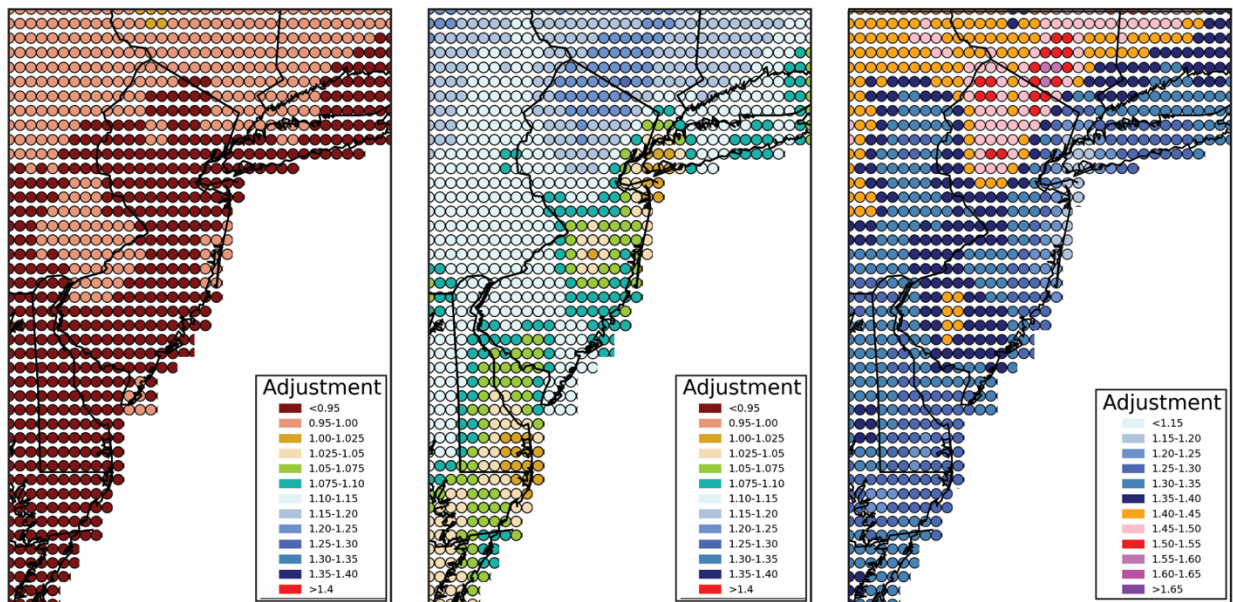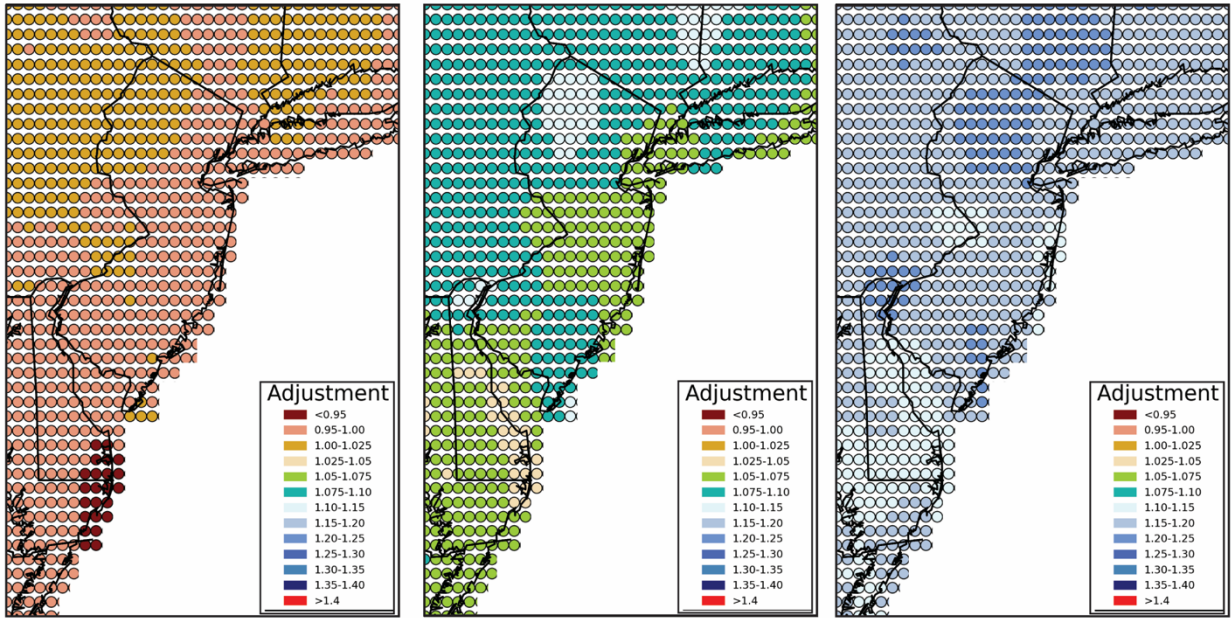*Figure 37. As in Figure 36, but for the 10-yr ARI.*
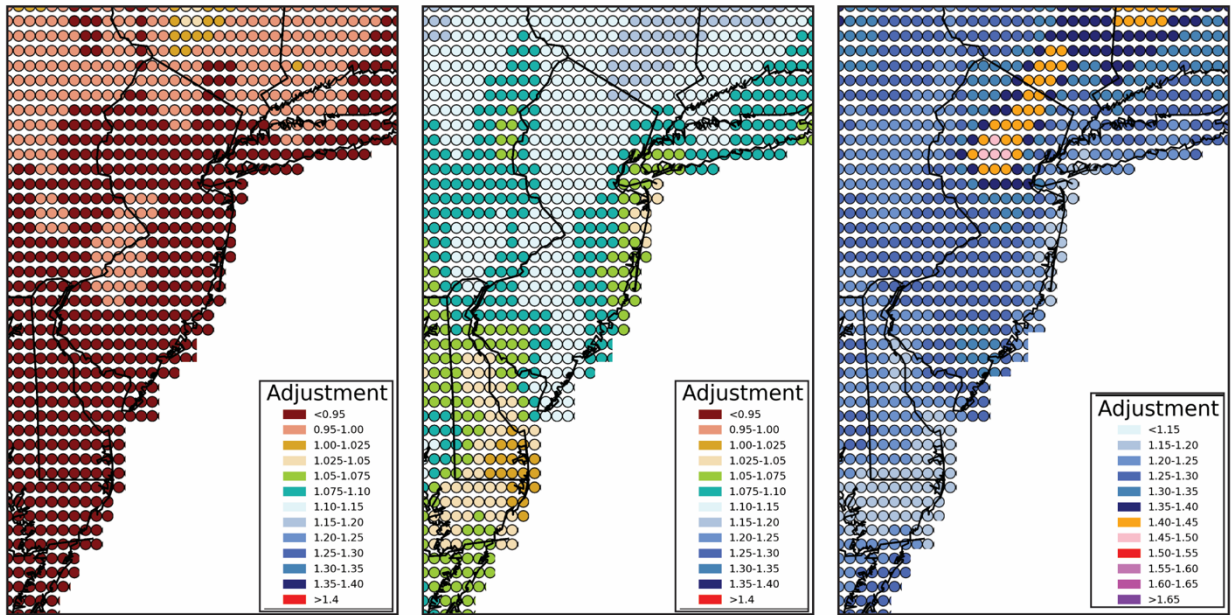
Figure 38. As in Figure 36, but for the 100-yr ARI.

iv.   Sub-daily change factors

A few studies have shown that sub-daily rainfall extremes might intensify at a higher rate than daily extremes (Prein et al. 2017). However, available climate model simulations are limited. Sub-daily data are only available from six of the 16 RCP 8.5 CORDEX simulations and are not a part of the LOCA dataset. This small subset of hourly projections is characterized by considerable between-model and between-station variability. In Figures 21-23, CFs based on daily CORDEX simulations are constrained between 0.8 and 2.0 for the 2- and 10-yr ARI and between 0.75 and 2.5 for the 100-yr ARI. In the hourly simulations, however, the range of hourly change factors is substantially larger, varying from > 2.5 to <0.50 for the 100-yr ARI (Fig. 39). For 3-hourly precipitation, the range of CF values narrows to a range similar to that of the daily values (Fig 39). These large differences coupled with the small number of available simulations, impedes the application of change factors at the sub-daily scale.

Despite this variability, the median CFs for the sub-daily durations were similar to the daily values.   Using only those datasets with hourly or 3-hourly simulations, there is little difference the median CF for 1-, 3-, 6-, 12- or 24-hr precipitation for the 2-, 10- and 100-yr ARI (Fig. 39). These median CF are also similar to those based on the larger set of daily resolution simulations, generally falling in the range of 10-30% (compare Figure 39 with Figures 21-23). Although in Figure 39, there is some evidence for a slight increase in median CF with decreasing hourly duration, due to the general consistency of the median, high variation among models and stations, and limited number of simulations, the more robust set
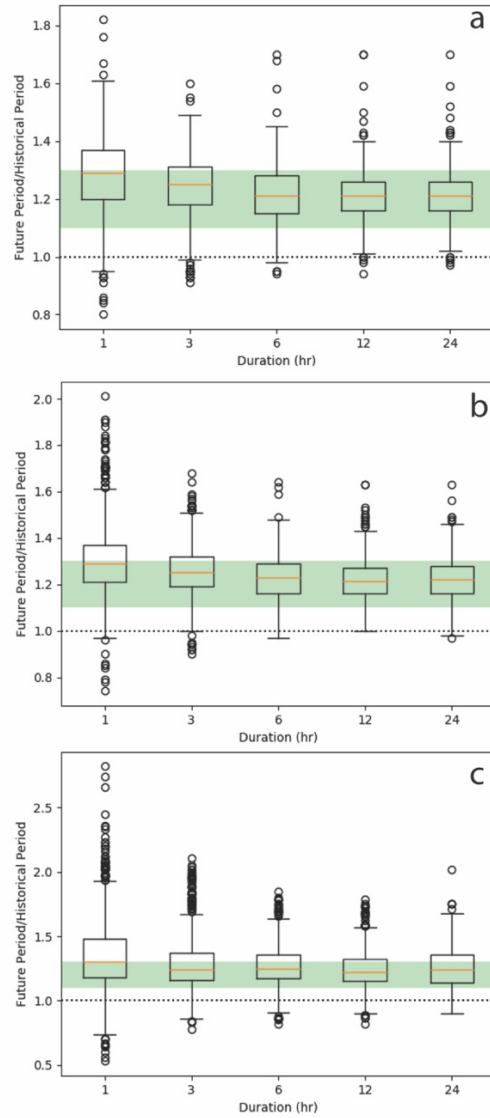
Figure 39. Boxplots of the median a) 2-yr, b) 10-yr and c) 100-yr ARI CORDEX change factors associated with various hourly durations.

of daily CFs are assumed to apply to sub-daily precipitation. This approach was also applied to future extreme rainfall projections for New York (DeGaetano and Castellano 2017) and for simulations covering the Virginia and locations within the Chesapeake Bay Watershed (Miro et al., 2021). Further support for the use of a static CF across sub-daily precipitation durations, is

provided by observational precipitation which shows similar increasing trends in ARI

precipitation amounts from 1990-2019 for different durations (DeGaetano and Tran, 2021).

Future refinement of the CFs associated with sub-daily precipitation extremes will be

warranted when a larger sample of higher temporal and spatial resolution model simulations

becomes available. In the current generation of climate model simulations processes such as

convection that typically generate extreme sub-daily rainfall rates are parameterized instead of

explicitly modeled, which further complicates the development of CFs for hourly precipitation

extremes.

5. Summary

A suite of 47 downscaled climate model simulations was used to estimate changes in

extreme rainfall amounts corresponding to the 2-, 5- 10-, 25-, 50- and 100-year ARI for locations

encompassing the state of New Jersey. Daily precipitation amounts from each climate model

were analyzed based on the approach used with observed data in NOAA Atlas 14. This allowed

the generation of ARI precipitation amounts for each model that corresponded to three 50-year

time periods. The historical period, 1950-1999, reflected the available data record at the

majority of stations in NOAA atlas 14, while providing a robust sample size for extreme value

analysis. Future simulations covered near term 2020-2069 and end-of-century 2050-2099

periods. Change factors (CF) representing the ratio of the future to historical values were then

computed.

Once interpolated to a common grid, the set of extreme precipitation CFs was pooled

across the ensemble of models and the median value retained for each grid point. In practice,

this value can be multiplied by the extreme rainfall reported for a location in Atlas 14 to obtain

an estimate of the magnitude of future extreme rainfall. Percentiles other than the median were

also extracted to provide a measure of uncertainty. The 17th-83rd percentile range was specifically chosen to reflect the "likely" range of future CFs.

Figure 40 summarizes the median CFs for the 2-, 10- and 100-yr ARI during the 2050-2099 and 2020-2069 periods under RCP 8.5 and RCP4.5. In general, the CF values show a similar spatial pattern of larger increases in the northern part of NJ and small increases in central NJ, along the coast, and farther south over Delaware, especially for the 100-yr ARI. Under a higher RCP 8.5 emissions scenario, rainfall extremes increase by between 10 and 30% across much of the state (CFs between 1.10 and 1.30) at the end of the century. In the interim 2020-2069 period, the change is more commonly in the 7.5-15% range. Although the 100-yr ARI in northern NJ, increases by as much as 20%.

Under more moderate RCP4.5 emissions, the change in the 2- and 10-yr ARI by the end of the century (2050-2099) is in line with the change for higher emissions in the earlier 2020-2070, typically an increase of between 7.5 and 15%. Under RCP 4.5 100-yr ARI precipitation in the 2050-2099 period changes very little from the current value (i.e. CF = 1.00) in the vicinity of New York City, with small 2.5-10% increases in central New Jersey and along the coast and larger 20-25% increases in northern NJ. Across the state, the 2-yr ARI increases by 5-7.5% , the 10-yr ARI increases by 5-15%, and increases in the 100-yr ARI range from 2.5% to 20% during the 2020-2069 period under moderate RCP 4.5 emissions.

Collectively the CF values computed in this study synthesize projections from a combination of the latest and most widely available generation of global climate model
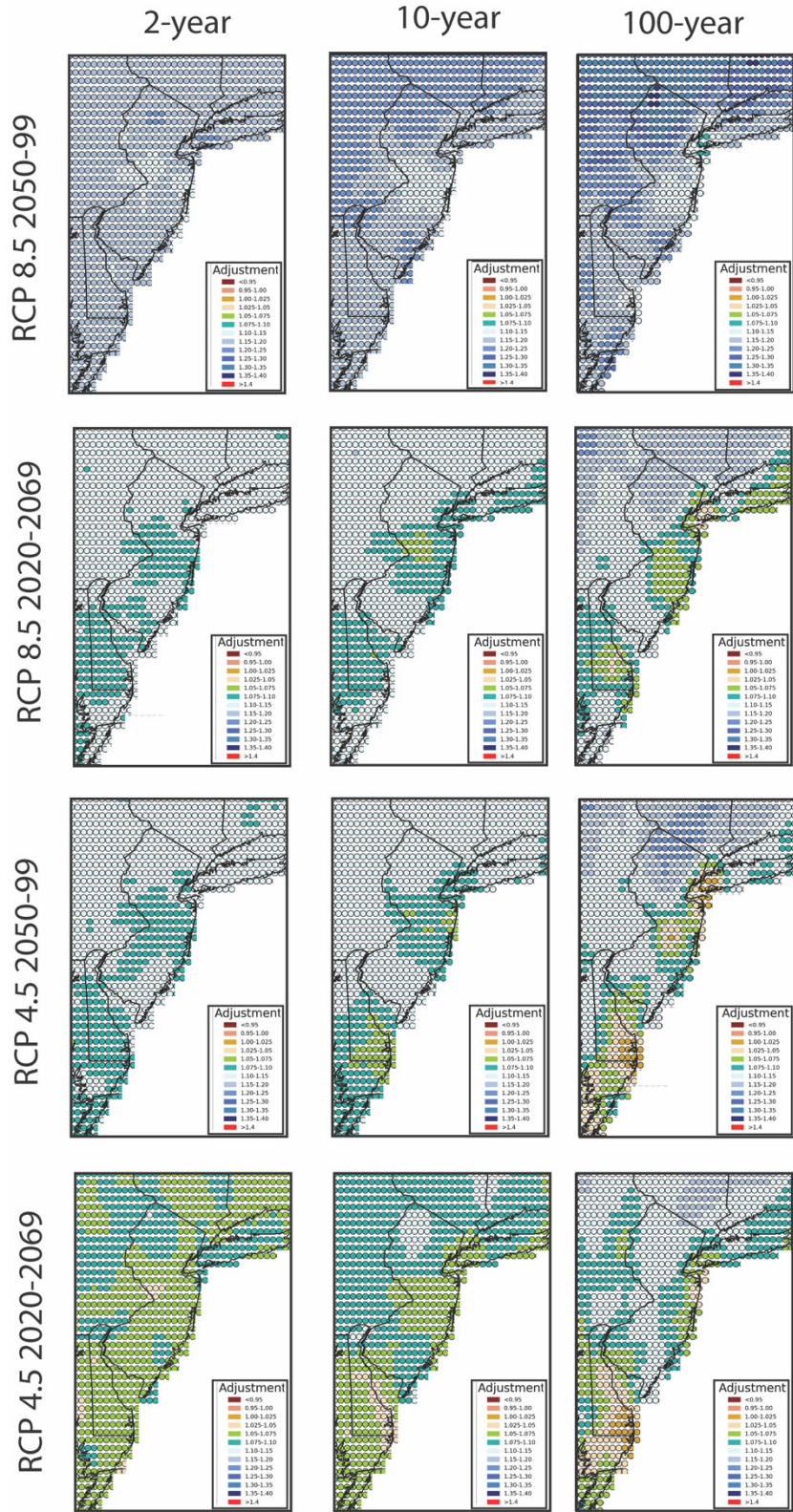
Figure 40. Median 2-yr, 10-yr and 100-yr ARI precipitation CF for 2050-2099 and 2020-2069 under RCP8.5 and RCP 4.5.

simulations and downscaling techniques. These data sets were selected based on their common

usage and ability to simulate and project rainfall extremes. They represent the best available

climate informed information on future changes in extreme rainfall. Nonetheless, these

projections are likely to evolve as newer climate models with enhanced resolution and improved

representation of heavy rainfall generation mechanisms are developed and improved

downscaling methodologies become available.

Future updates to these CFs are indicated to assure that the most relevant and reliable

climate data are being used in design and resiliency planning. A cursory examination of a

limited number of global scale simulations from the newest CMIP6 generation of models,

indicated CFs of similar magnitudes to those based on GCM-scale CMIP5 simulations under

RCP 8.5 during the 2050-2099 period (Fig. 41). In general, for both CMIP5 and CMIP6 the

model median CFs are for points encompassing NJ are in the range of 1.10-1.30 and show

similar variation. While this gives some indication that CFs based on the newer generation of

global models will be similar to those shown here, especially when accounting for the range of

uncertainty in the downscaled CMIP5 simulations, it will be prudent to reevaluate the CFs once

multiple sets of downscaled CMIP6 model projections become available.
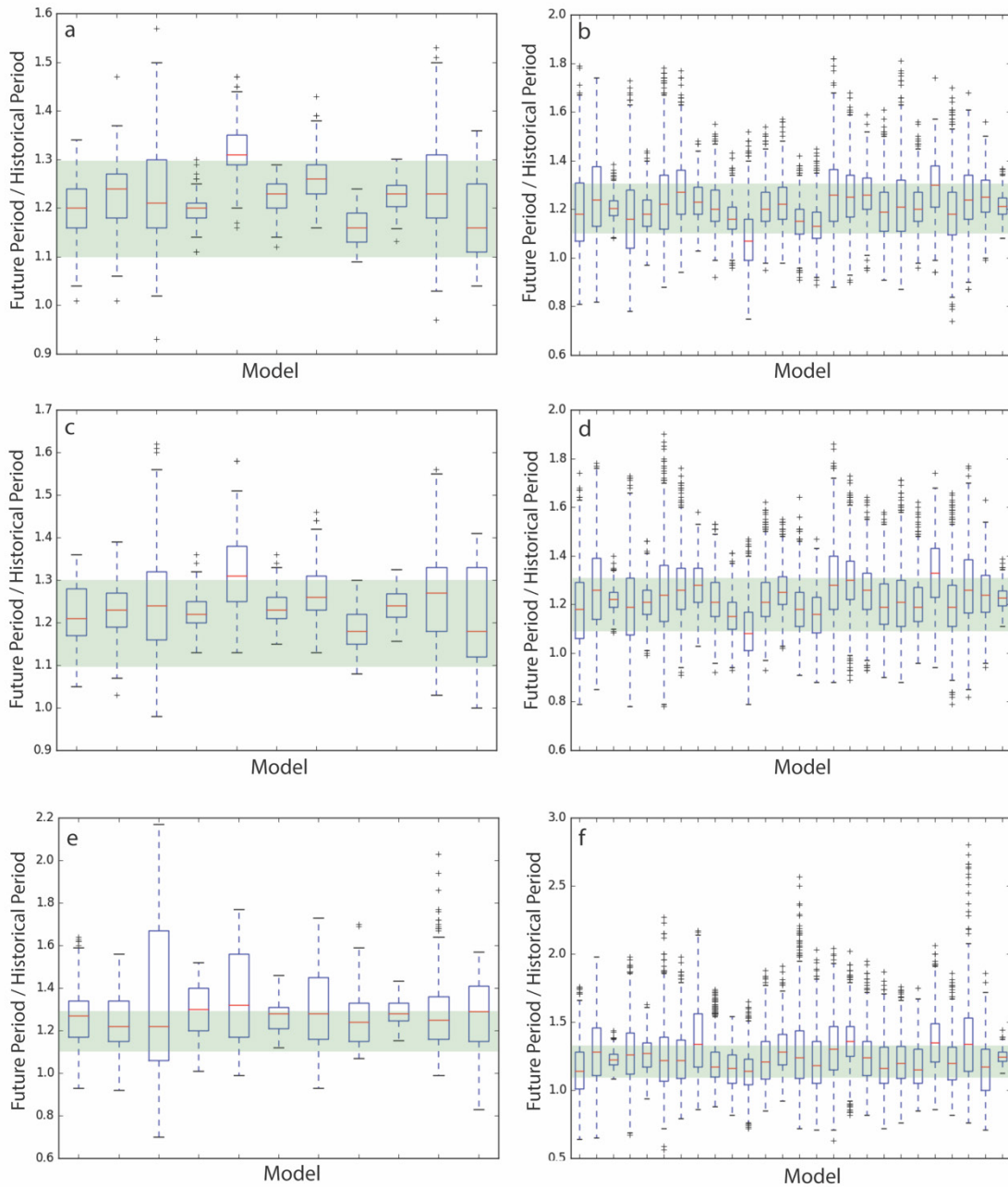
Figure 41. Change in a) 2-yr, c) 10-yr and e)100-yr ARI precipitation in 2050-2099 under RCP 8.5 relative to the 1950-1999 historical period for a subset of GCM-scale CMIP6 models. Analogous values for a set of GCM-scale CMIP5 model simulations are given for b) 2-yr, d) 10-yr and f) 100-yr ARI precipitation.

6. Acknowledgements

7. References

Abatzoglou J.T. and Brown T.J. 2012. "A comparison of statistical downscaling methods suited for wildfire applications". *International Journal of Climatology*, 32, 772-780. http://onlinelibrary.wiley.com/doi/10.1002/joc.2312/full

Agilan, V, and Umamahesh, N.V. 2017. "What Are the Best Covariates for Developing Non-Stationary Rainfall Intensity-Duration-Frequency Relationship?" Advances in Water Resources 101 (March): 11–22. https://doi.org/10.1016/j.advwatres.2016.12.016.

Armstrong, W.H., Collins, M.J. and Snyder, N.P. 2014: Hydroclimatic flood trends in the Northeastern United States and linkages with large-scale atmospheric circulation patterns. *Hydrological Sciences Journal*, **59**, 1636–1655, https://doi.org/10.1080/02626667.2013.862339

Bonnin, G.M., Martin, D., Lin, B., et al. 2006. NOAA Atlas 14: Precipitation-Frequency Atlas of the United States, volume 2, Version 3.0. ftp://ftp.library.noaa.gov/noaa_documents.lib/NWS/NOAA_Atlas/NOAA_Atlas_14/Atlas14_Volume2.pdf

Brown, V.M., B.D. Keim, and A.W. Black, 2020: Trend analysis of multiple extreme hourly precipitation time series in the southeast United States. *J. Appl. Meteor. Climatol.* **59(3)**, 427-442.

Cheng, Linyin, and A. AghaKouchak. 2014. "Nonstationary Precipitation Intensity-Duration-Frequency Curves for Infrastructure Design in a Changing Climate." Scientific Reports 4 (November). https://doi.org/10.1038/srep07093.

Collins, M.J., 2009: Evidence for changing flood risk in New England since the late 20th century. *Journal of the American Water Resources Association (JAWRA)* **45(2)**, 279-290, doi: 10.1111/j.1752-1688.2008.00277.

Collins, M., *et al.* (2013) Section 12.3.1.3 The New Concentration Driven RCP Scenarios, and their Extensions, in: Chapter 12: Long-term Climate Change: Projections, Commitments and Irreversibility (archived 16 July 2014), in: IPCC AR5 WG1 2013, pp. 1045-1047

Cook, L.M., C.J. Anderson, and C. Samaras. 2017. "Framework for Incorporating Downscaled Climate Output into Existing Engineering Methods: Application to Precipitation Frequency

Curves." Journal of Infrastructure Systems 23 (4): 04017027. https://doi.org/10.1061/(ASCE)IS.1943-555X.0000382.

Cooley, A. and H. Chang, 2017: Precipitation intensity trend detection using hourly and daily observations in Portland, Oregon. *Climate*, *5(1)*, 2-17.

Coumou, D., and S. Rahmstorf, 2012: A decade of weather extremes. *Nature Climate Change*, **2**, 491-496.

DeGaetano, A.T., 2009: Time-dependent changes in extreme-precipitation return-period amounts in the continental United States. *J. Appl. Meteor. Climatol.*, **48**, 2086–2099.

DeGaetano, Arthur T., and C. M. Castellano. 2017. "Future Projections of Extreme Precipitation Intensity-Duration-Frequency Curves for Climate Adaptation Planning in New York State." Climate Services 5 (January): 23–35. https://doi.org/10.1016/j.cliser.2017.03.003.

DeGaetano, A.T. and Castellano, C., 2018. Selecting time series length to moderate the impact of nonstationarity in extreme rainfall analyses. Journal of Applied Meteorology and Climatology, 57(10), pp.2285-2296.

Donat, M.G., A.L. Lowry, L.V. Alexander, P.A. O'Gorman, and N. Maher, 2016: More extreme precipitation in the world's dry and wet regions. *Nature Climate Change*, **6**, 508-513.

Eum, H.I. and Cannon, A.J., 2017. Intercomparison of projected changes in climate extremes for South Korea: application of trend preserving statistical downscaling methods to the CMIP5 ensemble. *International Journal of Climatology*, *37*(8), pp.3381-3397.

Fischer, E. M. and R. Knutti, 2016: Observed heavy precipitation increase confirms theory and early models. *Nature Climate Change*, 6(11), 986–991, http://doi.org/10.1038/nclimate3110.

Georgakakos, A., P. Fleming, M. Dettinger, C. Peters-Lidard, T.C., Richmond, K. Reckhow, K. White, and D. Yates, 2014: Water resources, in *Climate Change Impacts in the United States: The Third National Climate Assessment. Global Change Res. Program,* Washington, D.C., 69-112.

Groisman, P.Y., 1992: Studying the North American precipitation changes during the last 100 years. In *Proc. of the 5th Int. Meeting on Statistical Climatology, Toronto, Amer. Meteor. Soc* 75-79.

Groisman, P. Ya., R.W. Knight, D.R. Easterling, T.R. Karl, G.C. Hegerl, and V.N. Razuvaev, 2005: Trends in intense precipitation in the climate record. *J. Climate*, **18**, 1343–1367.

Groisman, P. Ya., R. W. Knight, and T. R. Karl, 2012: Changes in intense precipitation over the central United States. *J. Hydrometeor.*, **13**, 47–66.

Heineman, M., 2012: Trends in precipitation maxima at US Historical Climatology Network Stations: 1893-2010. In *World Environmental and Water Resources Congress 2012: Crossing Boundaries*, 2003-2012.

Hosking, J. 1990. L-Moments: Analysis and Estimation of Distributions Using Linear Combinations of Order Statistics. Journal of the Royal Statistical Society. Series B (Methodological),52(1), 105-124.

Kenyon, J., and G.C. Hegerl, 2010. Influence of modes of climate variability on global precipitation extremes. *J. Climate*, *23*(23), 6248-6262.

Kunkel, K.E., 2003: North American trends in extreme precipitation. *Natural hazards*, *29***(2)**, 291-305.

Kunkel, K.E., K. Andsager, and D.R. Easterling, 1999. Long-term trends in extreme precipitation events over the conterminous United States and Canada. *J. Climate*, *12***(8)**, 2515-2527.

Kunkel, K.E., Easterling, D.R., Kristovich, D.A., Gleason, B., Stoecker, L. and Smith, R., 2010. Recent increases in US heavy precipitation associated with tropical cyclones. *Geophysical Research Letters*, *37*(24).

Kunkel K., and Coauthors, 2013: Regional climate trends and scenarios for the U.S. National Climate Assessment: Part 1—Climate of the Northeast U.S. NOAA Tech. Rep. NESDIS 142-1, 80 pp. [Available online at https://www.nesdis.noaa.gov/sites/default/files/asset/document/NOAA_NESDIS_Tech_Report_142-1-Climate_of_the_Northeast_US.pdf.]

Lenderink, G., H.Y. Mok, T.C. Lee, and G.J. Van Oldenborgh, 2011: Scaling and trends of hourly precipitation extremes in two different climate zones–Hong Kong and the Netherlands. *Hydrology and Earth System Sciences*, *15***(9)**, 3033-3041.

López-Cantú, T., Prein, A.F. and Samaras, C., 2020. Uncertainties in future US extreme precipitation from downscaled climate projections. Geophysical Research Letters, 47(9), p.e2019GL086797.

Madsen, H., P.F. Rasmussen, and D. Rosbjerg. 1997. "Comparison of Annual Maximum Series and Partial Duration Series Methods for Modeling Extreme Hydrologic Events: 1. At-Site Modeling." *Water Resources Research* 33 (4): 747–57. https://doi.org/10.1029/96WR03848.

Maraun, D., Wetterhall, F., Ireson, A.M., Chandler, R.E., Kendon, E.J., Widmann, M., Brienen, S., Rust, H.W., Sauter, T., Themeßl, M. and Venema, V.K.C., 2010. Precipitation downscaling under climate change: Recent developments to bridge the gap between dynamical models and the end user. *Reviews of geophysics*, *48*(3). https://doi.org/10.1029/2009RG000314)

Martins, E.S., and J.R. Stedinger. 2000. "Generalized Maximum-Likelihood Generalized Extreme-Value Quantile Estimators for Hydrologic Data." *Water Resources Research* 36 (3): 737–44. https://doi.org/10.1029/1999WR900330.

Mastrandrea, M.D., C.B. Field, T.F. Stocker, O. Edenhofer, K.L. Ebi, D.J. Frame, H. Held, E. Kriegler, K.J. Mach, P.R. Matschoss, G.-K. Plattner, G.W. Yohe, and F.W. Zwiers, 2010: *Guidance Note for Lead Authors of the IPCC Fifth Assessment Report on Consistent Treatment of Uncertainties.* Intergovernmental Panel on Climate Change (IPCC). Available at <http://www.ipcc.ch>.

Mearns, L.O., et al. 2017. "The NA-CORDEX dataset, version 1.0." NCAR Climate Data Gateway, Boulder CO, https://doi.org/10.5065/D6SJ1JCH

Miro, M.E., A.T. DeGaetano, T. López-Cantú, C. Samaras, M. Webber, and K. Romita Grocholski, 2021: Developing Future Projected Intensity- Duration-Frequency (IDF) Curves: A Technical Report on Data, Methods and IDF Curves for the Chesapeake Bay Watershed and Virginia, Rand Corporation Technical Report TL-A1365-1, 50 pp. [https://midatlantic-idf.rcc-acis.org].

Ning, L., E.E. Riddle, and R.S. Bradley, 2015: Projected changes in climate extremes over the northeastern United States. *J. Climate*, **28**, 3289-3310.

Papalexiou, S.M. and Koutsoyiannis, D., 2013. Battle of extreme value distributions: A global survey on extreme daily rainfall. Water Resources Research, 49(1), pp.187-201.

Perica, S., Pavlovic, S., St Laurent, M., Trypaluk, C., Unruh, D., Martin, D. and Wilhite, O., 2015. Precipitation-Frequency Atlas of the United States. Volume 10, Version 3.0. Northern States; Connecticut, Maine, Massachusetts, New Hampshire, New York, Rhode Island, Vermont.

Peterson, T., R. and Co-authors, 2013: Monitoring and understanding changes in heat waves, cold waves, floods and droughts in the United States: State of knowledge. *Bulletin of the American Meteorological Society*, *94*(6), 821-834.

Pierce, D.W., Cayan, D.R. and B.L. Thrasher. 2014. "Statistical downscaling using Localized Constructed Analogs (LOCA)." Journal of Hydrometeorology, volume 15, page 2558-2585. http://journals.ametsoc.org/doi/abs/10.1175/JHM-D-14-0082.1

Prein, A.F., R.M. Rasmussen, K. Ikeda, C. Liu, M.P. Clark, and G.J. Holland. 2017. "The Future Intensification of Hourly Precipitation Extremes." *Nature Climate Change* 7 (1): 48–52.

Ragno, E., A. AghaKouchak, C.A. Love, L. Cheng, F. Vahedifard, and C. HR Lima. 2018. "Quantifying Changes in Future Intensity-Duration-Frequency Curves Using Multimodel Ensemble Simulations." Water Resources Research 54 (3): 1751–64.

Sarhadi, A., and E.D. Soulis. 2017. "Time-Varying Extreme Rainfall Intensity-Duration-Frequency Curves in a Changing Climate." Geophysical Research Letters 44 (5): 2454–63. https://doi.org/10.1002/2016GL072201.

Sun, Q., C. Miao, and Q. Duan, 2016: Extreme climate events and agricultural climate indices in China: CMIP5 model evaluation and projections. *Int. J. Climatol.*, **36**, 43–61. doi:10.1002/joc.4328.

Thakali, R., A. Kalra, and S. Ahmad. 2016. "Understanding the Effects of Climate Change on Urban Stormwater Infrastructures in the Las Vegas Valley." Hydrology 3 (4): 34. https://doi.org/10.3390/hydrology3040034.

Walsh, J., and Co-authors, 2014: "Ch. 2: Our Changing Climate." Climate Change Impacts in the United States: The Third National Climate Assessment, J.M. Melillo, Terese (T.C.) Richmond, and G.W. Yohe, Eds., U.S. Global Change Research Program, 19-67. doi:10.7930/J0KW5CXT

Wright, Daniel B., Christopher D. Bosma, and Tania Lopez-Cantu. 2019. "U.S. Hydrologic Design Standards Insufficient Due to Large Increases in Frequency of Rainfall Extremes." *Geophysical Research Letters* 46 (14): 8144–53. https://doi.org/10.1029/2019GL083235.

Wu, S., Markus, M., Lorenz, D., Angel, J.R. and Grady, K., 2019. "A Comparative Analysis of the Historical Accuracy of the Point Precipitation Frequency Estimates of Four Data Sets and Their Projections for the Northeastern United States." Water 11 (6): 1279. https://doi.org/10.3390/w11061279.

USGCRP, 2018: *Impacts, Risks, and Adaptation in the United States: Fourth National Climate Assessment, Volume II* [Reidmiller, D.R., C.W. Avery, D.R. Easterling, K.E. Kunkel, K.L.M. Lewis, T.K. Maycock, and B.C. Stewart (eds.)]. U.S. Global Change Research Program, Washington, DC, USA, 1515 pp. doi: 10.7930/NCA4.2018.

Yan, Hongxiang, Ning Sun, Xiaodong Chen, and Mark Wigmosta. 2020. "Next-Generation Intensity-Duration-Frequency Curves for Climate-Resilient Infrastructure Design: Advances and Opportunities." *Frontiers in Water* 2 (December): 545051. https://doi.org/10.3389/frwa.2020.545051.

SEE EXCEL TABLES FOR CURRENT DATA TABLE A1. County-based 2-yr ARI change factors and projected precipitation estimates for 2050-2099 under RCP8.5 emissions.

County	Change Factor				Projected Precipitation		
	17th Percentile	Median	83rd Percentile		17th Percentile	Median	83rd Percentile
Atlantic	1.09	1.18	1.30		3.60	3.91	4.29
Bergen	1.10	1.19	1.30		3.64	3.95	4.30
Burlington	1.07	1.15	1.24		3.59	3.88	4.19
Camden	1.07	1.16	1.26		3.55	3.82	4.15
Cape May	1.08	1.18	1.30		3.47	3.78	4.18
Cumberland	1.08	1.17	1.28		3.50	3.81	4.16
Essex	1.08	1.16	1.29		3.66	3.96	4.37
Gloucester	1.07	1.16	1.27		3.52	3.81	4.18
Hudson	1.08	1.17	1.28		3.55	3.85	4.22
Hunterdon	1.07	1.16	1.27		3.63	3.94	4.31
Mercer	1.05	1.13	1.23		3.47	3.76	4.08
Middlesex	1.07	1.16	1.27		3.56	3.86	4.24
Monmouth	1.07	1.16	1.27		3.62	3.91	4.29
Morris	1.09	1.20	1.33		3.89	4.27	4.72
Ocean	1.08	1.16	1.26		3.72	4.00	4.35
Passaic	1.09	1.19	1.31		3.74	4.07	4.49
Salem	1.07	1.17	1.30		3.50	3.83	4.24
Somerset	1.06	1.16	1.28		3.48	3.82	4.21
Sussex	1.09	1.20	1.31		3.47	3.80	4.16
Union	1.08	1.17	1.30		3.66	3.98	4.42
Warren	1.07	1.16	1.27		3.58	3.88	4.23

SEE EXCEL TABLES FOR CURRENT DATA TABLE A2. County-based 10-yr ARI change factors and projected precipitation estimates for 2050-2099 under RCP8.5 emissions.

County	Change Factor				Projected Precipitation		
	17th Percentile	Median	83rd Percentile		17th Percentile	Median	83rd Percentile
Atlantic	1.07	1.20	1.34		5.49	6.16	6.88
Bergen	1.08	1.20	1.33		5.45	6.06	6.71
Burlington	1.05	1.14	1.27		5.44	5.91	6.60
Camden	1.07	1.18	1.29		5.40	5.94	6.54
Cape May	1.08	1.21	1.34		5.38	6.04	6.69
Cumberland	1.07	1.18	1.31		5.39	5.99	6.63
Essex	1.06	1.18	1.32		5.52	6.12	6.86
Gloucester	1.07	1.19	1.31		5.42	5.99	6.60
Hudson	1.05	1.16	1.30		5.23	5.75	6.46
Hunterdon	1.07	1.19	1.32		5.37	6.00	6.64
Mercer	1.03	1.12	1.27		5.17	5.59	6.33
Middlesex	1.05	1.15	1.30		5.35	5.88	6.62
Monmouth	1.05	1.15	1.28		5.46	6.01	6.69
Morris	1.09	1.24	1.39		5.73	6.51	7.27
Ocean	1.06	1.14	1.28		5.68	6.15	6.89
Passaic	1.09	1.22	1.37		5.64	6.33	7.06
Salem	1.07	1.20	1.33		5.37	6.04	6.67
Somerset	1.06	1.20	1.33		5.24	5.92	6.59
Sussex	1.10	1.25	1.38		5.07	5.78	6.38
Union	1.07	1.19	1.33		5.54	6.19	6.91
Warren	1.08	1.21	1.33		5.26	5.92	6.49

SEE EXCEL TABLES FOR CURRENT DATA TABLE A3. County-based 100-yr ARI change factors and projected precipitation estimates for 2050-2099 under RCP8.5 emissions.

County	Change Factor				Projected Precipitation		
	17th Percentile	Median	83rd Percentile		17th Percentile	Median	83rd Percentile
Atlantic	0.94	1.22	1.47		8.37	10.86	13.05
Bergen	1.01	1.24	1.46		8.43	10.36	12.27
Burlington	0.96	1.13	1.40		8.51	9.99	12.39
Camden	0.98	1.22	1.44		8.31	10.33	12.22
Cape May	0.98	1.19	1.46		8.44	10.25	12.53
Cumberland	0.95	1.18	1.47		8.26	10.27	12.82
Essex	0.97	1.21	1.44		8.45	10.53	12.51
Gloucester	0.96	1.22	1.46		8.24	10.43	12.45
Hudson	0.92	1.13	1.37		7.54	9.25	11.26
Hunterdon	0.99	1.26	1.50		7.92	10.15	12.04
Mercer	0.96	1.17	1.43		7.90	9.70	11.79
Middlesex	0.95	1.17	1.42		8.17	10.05	12.28
Monmouth	0.96	1.16	1.38		8.52	10.33	12.32
Morris	1.04	1.31	1.52		8.66	10.96	12.69
Ocean	0.96	1.14	1.34		8.88	10.54	12.39
Passaic	1.04	1.32	1.55		8.87	11.21	13.17
Salem	0.97	1.19	1.42		8.25	10.14	12.14
Somerset	0.99	1.28	1.53		8.00	10.40	12.44
Sussex	1.07	1.36	1.60		8.04	10.14	11.98
Union	0.96	1.21	1.44		8.41	10.59	12.55
Warren	1.01	1.28	1.51		7.88	10.02	11.83

SEE EXCEL TABLES FOR CURRENT DATA TABLE B1. County-based 2-yr ARI change factors and projected precipitation estimates for 2050-2099 under RCP4.5 emissions.

County	Change Factor				Projected Precipitation		
	17th Percentile	Median	83rd Percentile		17th Percentile	Median	83rd Percentile
Atlantic	1.03	1.11	1.22		3.39	3.67	4.03
Bergen	1.04	1.11	1.20		3.45	3.69	3.96
Burlington	1.01	1.09	1.17		3.41	3.67	3.95
Camden	1.02	1.09	1.18		3.36	3.60	3.88
Cape May	1.02	1.11	1.21		3.27	3.57	3.89
Cumberland	1.02	1.11	1.20		3.32	3.61	3.90
Essex	1.01	1.09	1.19		3.43	3.72	4.05
Gloucester	1.01	1.09	1.19		3.33	3.59	3.89
Hudson	1.02	1.10	1.19		3.35	3.61	3.92
Hunterdon	1.02	1.10	1.19		3.47	3.74	4.03
Mercer	1.00	1.08	1.16		3.33	3.58	3.84
Middlesex	1.00	1.09	1.19		3.34	3.66	3.97
Monmouth	1.01	1.09	1.19		3.42	3.70	4.01
Morris	1.05	1.12	1.23		3.74	4.00	4.36
Ocean	1.03	1.09	1.18		3.54	3.78	4.06
Passaic	1.04	1.12	1.21		3.58	3.83	4.14
Salem	1.01	1.11	1.20		3.30	3.60	3.92
Somerset	1.01	1.10	1.19		3.32	3.60	3.91
Sussex	1.06	1.13	1.24		3.35	3.60	3.93
Union	1.01	1.10	1.20		3.43	3.72	4.08
Warren	1.04	1.11	1.20		3.48	3.71	4.00

SEE EXCEL TABLES FOR CURRENT DATA TABLE B2. County-based 10-yr ARI change factors and projected precipitation estimates for 2050-2099 under RCP4.5 emissions.

County	Change Factor				Projected Precipitation		
	17th Percentile	Median	83rd Percentile		17th Percentile	Median	83rd Percentile
Atlantic	1.01	1.11	1.24		5.20	5.73	6.38
Bergen	1.03	1.12	1.23		5.19	5.64	6.19
Burlington	1.00	1.08	1.18		5.22	5.62	6.15
Camden	1.02	1.11	1.22		5.15	5.58	6.16
Cape May	1.03	1.12	1.24		5.14	5.59	6.19
Cumberland	1.02	1.11	1.21		5.16	5.60	6.11
Essex	1.01	1.10	1.22		5.22	5.70	6.31
Gloucester	1.02	1.11	1.23		5.14	5.60	6.19
Hudson	0.99	1.08	1.19		4.94	5.38	5.92
Hunterdon	1.03	1.10	1.23		5.17	5.53	6.18
Mercer	0.99	1.07	1.17		4.96	5.37	5.87
Middlesex	0.98	1.08	1.21		5.02	5.53	6.20
Monmouth	0.99	1.08	1.19		5.14	5.62	6.19
Morris	1.05	1.14	1.28		5.49	5.99	6.73
Ocean	1.00	1.09	1.19		5.40	5.85	6.38
Passaic	1.04	1.14	1.27		5.38	5.89	6.55
Salem	1.02	1.12	1.23		5.13	5.61	6.16
Somerset	1.02	1.11	1.24		5.03	5.48	6.14
Sussex	1.05	1.15	1.29		4.84	5.30	5.97
Union	1.01	1.10	1.23		5.22	5.70	6.39
Warren	1.04	1.12	1.25		5.11	5.49	6.12

SEE EXCEL TABLES FOR CURRENT DATA TABLE B3. County-based 100-yr ARI change factors and projected precipitation estimates for 2050-2099 under RCP4.5 emissions.

County	Change Factor				Projected Precipitation		
	17th Percentile	Median	83rd Percentile		17th Percentile	Median	83rd Percentile
Atlantic	0.85	1.10	1.39		7.53	9.78	12.35
Bergen	0.96	1.15	1.37		8.01	9.67	11.44
Burlington	0.92	1.06	1.32		8.14	9.42	11.66
Camden	0.96	1.14	1.39		8.09	9.64	11.74
Cape May	0.95	1.13	1.32		8.17	9.71	11.37
Cumberland	0.85	1.06	1.39		7.44	9.23	12.12
Essex	0.94	1.12	1.33		8.19	9.70	11.56
Gloucester	0.95	1.14	1.41		8.14	9.73	12.03
Hudson	0.92	1.04	1.23		7.53	8.56	10.08
Hunterdon	0.91	1.13	1.42		7.34	9.06	11.43
Mercer	0.92	1.09	1.36		7.64	8.98	11.21
Middlesex	0.88	1.10	1.33		7.60	9.48	11.47
Monmouth	0.92	1.07	1.26		8.20	9.51	11.25
Morris	0.95	1.20	1.46		7.91	10.00	12.19
Ocean	0.94	1.07	1.24		8.68	9.97	11.50
Passaic	0.93	1.22	1.50		7.95	10.39	12.78
Salem	0.95	1.11	1.32		8.09	9.44	11.29
Somerset	0.93	1.17	1.48		7.58	9.48	11.98
Sussex	0.95	1.21	1.50		7.09	9.05	11.22
Union	0.93	1.11	1.35		8.13	9.72	11.79
Warren	0.95	1.15	1.37		7.42	8.98	10.70

SEE EXCEL TABLES FOR CURRENT DATA TABLE C1. County-based 2-yr ARI change factors and projected precipitation estimates for 2020-2069 under RCP8.5 emissions.

County	Change Factor				Projected Precipitation		
	17th Percentile	Median	83rd Percentile		17th Percentile	Median	83rd Percentile
Atlantic	1.00	1.11	1.21		3.31	3.66	3.98
Bergen	1.01	1.12	1.22		3.34	3.71	4.02
Burlington	1.00	1.09	1.18		3.38	3.68	3.99
Camden	1.00	1.10	1.19		3.31	3.62	3.93
Cape May	0.99	1.10	1.20		3.18	3.53	3.85
Cumberland	1.00	1.10	1.20		3.25	3.59	3.90
Essex	0.99	1.10	1.20		3.37	3.73	4.09
Gloucester	1.00	1.10	1.20		3.28	3.61	3.93
Hudson	1.00	1.10	1.20		3.28	3.62	3.95
Hunterdon	1.00	1.10	1.20		3.39	3.74	4.06
Mercer	0.99	1.08	1.17		3.30	3.59	3.90
Middlesex	0.98	1.10	1.20		3.29	3.66	3.99
Monmouth	1.00	1.10	1.20		3.36	3.71	4.05
Morris	1.00	1.12	1.24		3.57	4.00	4.40
Ocean	1.00	1.10	1.19		3.44	3.79	4.11
Passaic	1.00	1.12	1.22		3.44	3.83	4.19
Salem	1.00	1.11	1.21		3.26	3.61	3.94
Somerset	0.99	1.10	1.20		3.27	3.62	3.96
Sussex	1.02	1.13	1.23		3.22	3.58	3.90
Union	0.99	1.10	1.21		3.37	3.74	4.11
Warren	1.01	1.11	1.20		3.37	3.70	4.01

SEE EXCEL TABLES FOR CURRENT DATA TABLE C2. County-based 10-yr ARI change factors and projected precipitation estimates for 2020-2069 under RCP8.5 emissions.

County	Change Factor				Projected Precipitation		
	17th Percentile	Median	83rd Percentile		17th Percentile	Median	83rd Percentile
Atlantic	1.00	1.11	1.22		5.14	5.71	6.29
Bergen	1.01	1.11	1.23		5.08	5.62	6.21
Burlington	0.99	1.08	1.19		5.14	5.60	6.20
Camden	1.01	1.10	1.21		5.11	5.55	6.09
Cape May	1.00	1.11	1.21		4.99	5.52	6.06
Cumberland	1.00	1.11	1.21		5.08	5.62	6.15
Essex	0.99	1.10	1.22		5.12	5.70	6.35
Gloucester	1.01	1.11	1.21		5.10	5.57	6.09
Hudson	0.98	1.08	1.21		4.88	5.38	6.02
Hunterdon	1.01	1.11	1.23		5.05	5.58	6.20
Mercer	0.98	1.07	1.19		4.91	5.34	5.96
Middlesex	0.98	1.08	1.22		4.99	5.52	6.25
Monmouth	0.99	1.08	1.21		5.16	5.64	6.33
Morris	1.00	1.13	1.29		5.27	5.92	6.76
Ocean	1.00	1.09	1.20		5.37	5.84	6.46
Passaic	1.00	1.13	1.26		5.18	5.87	6.53
Salem	1.01	1.12	1.23		5.09	5.62	6.18
Somerset	0.99	1.11	1.24		4.92	5.48	6.15
Sussex	1.03	1.13	1.27		4.76	5.24	5.85
Union	0.98	1.10	1.23		5.11	5.70	6.40
Warren	1.02	1.12	1.24		4.98	5.46	6.09

SEE EXCEL TABLES FOR CURRENT DATA TABLE C3. County-based 100-yr ARI change factors and projected precipitation estimates for 2020-2069 under RCP8.5 emissions.

County	Change Factor				Projected Precipitation		
	17th Percentile	**Median**	**83rd Percentile**		**17th Percentile**	**Median**	**83rd Percentile**
Atlantic	0.92	1.09	1.32		8.18	9.72	11.70
Bergen	0.94	1.12	1.32		7.91	9.38	11.06
Burlington	0.90	1.06	1.26		8.00	9.43	11.19
Camden	0.94	1.12	1.28		8.00	9.47	10.84
Cape May	0.96	1.12	1.30		8.24	9.67	11.22
Cumberland	0.91	1.12	1.37		7.94	9.78	11.96
Essex	0.92	1.10	1.32		7.98	9.58	11.46
Gloucester	0.94	1.12	1.29		8.03	9.53	11.04
Hudson	0.88	1.06	1.26		7.24	8.67	10.31
Hunterdon	0.96	1.13	1.36		7.75	9.11	10.91
Mercer	0.92	1.09	1.28		7.60	8.97	10.58
Middlesex	0.90	1.08	1.29		7.77	9.35	11.11
Monmouth	0.91	1.09	1.28		8.12	9.68	11.45
Morris	0.95	1.18	1.44		7.90	9.80	12.00
Ocean	0.95	1.06	1.24		8.80	9.88	11.47
Passaic	0.95	1.17	1.44		8.10	10.00	12.23
Salem	0.96	1.11	1.30		8.20	9.44	11.08
Somerset	0.96	1.15	1.41		7.79	9.34	11.44
Sussex	0.99	1.19	1.44		7.41	8.93	10.75
Union	0.92	1.11	1.32		8.05	9.64	11.53
Warren	0.94	1.15	1.39		7.33	8.98	10.84

SEE EXCEL TABLES FOR CURRENT DATA TABLE D1. County-based 2-yr ARI change factors and projected precipitation estimates for 2020-2069 under RCP4.5 emissions.

County	Change Factor				Projected Precipitation		
	17th Percentile	Median	83rd Percentile		17th Percentile	Median	83rd Percentile
Atlantic	0.98	1.08	1.18		3.24	3.57	3.88
Bergen	0.99	1.07	1.16		3.28	3.56	3.85
Burlington	0.99	1.07	1.15		3.33	3.59	3.87
Camden	0.98	1.06	1.16		3.24	3.50	3.81
Cape May	0.98	1.07	1.17		3.15	3.45	3.76
Cumberland	0.99	1.07	1.16		3.20	3.47	3.77
Essex	0.98	1.07	1.16		3.33	3.62	3.94
Gloucester	0.97	1.06	1.16		3.20	3.48	3.79
Hudson	0.98	1.07	1.17		3.23	3.52	3.83
Hunterdon	0.99	1.07	1.17		3.34	3.63	3.97
Mercer	0.97	1.04	1.14		3.23	3.47	3.78
Middlesex	0.97	1.06	1.17		3.22	3.55	3.91
Monmouth	0.98	1.07	1.17		3.30	3.61	3.95
Morris	1.00	1.08	1.19		3.56	3.86	4.23
Ocean	0.99	1.06	1.15		3.42	3.66	3.96
Passaic	0.99	1.07	1.17		3.41	3.69	4.01
Salem	0.97	1.07	1.17		3.16	3.48	3.83
Somerset	0.97	1.07	1.17		3.20	3.51	3.86
Sussex	1.01	1.10	1.19		3.21	3.48	3.79
Union	0.97	1.07	1.17		3.31	3.63	3.98
Warren	1.01	1.08	1.16		3.36	3.60	3.88

SEE EXCEL TABLES FOR CURRENT DATA TABLE D2. County-based 10-yr ARI change factors and projected precipitation estimates for 2020-2069 under RCP4.5 emissions.

County	Change Factor				Projected Precipitation		
	17th Percentile	Median	83rd Percentile		17th Percentile	Median	83rd Percentile
Atlantic	1.00	1.09	1.19		5.13	5.62	6.13
Bergen	0.99	1.08	1.19		4.97	5.44	5.98
Burlington	0.99	1.07	1.16		5.13	5.55	6.03
Camden	1.00	1.08	1.17		5.05	5.43	5.91
Cape May	1.00	1.10	1.19		4.97	5.47	5.96
Cumberland	0.99	1.07	1.16		5.01	5.43	5.87
Essex	0.97	1.07	1.18		5.05	5.57	6.14
Gloucester	0.99	1.08	1.17		5.01	5.43	5.91
Hudson	0.97	1.07	1.17		4.82	5.31	5.81
Hunterdon	1.00	1.09	1.19		5.03	5.45	5.95
Mercer	0.99	1.06	1.14		4.93	5.29	5.68
Middlesex	0.97	1.07	1.19		4.96	5.46	6.06
Monmouth	0.97	1.06	1.17		5.05	5.54	6.10
Morris	1.01	1.10	1.24		5.30	5.78	6.49
Ocean	0.99	1.06	1.16		5.31	5.73	6.22
Passaic	1.00	1.09	1.22		5.15	5.64	6.28
Salem	0.98	1.09	1.19		4.93	5.45	5.99
Somerset	0.99	1.09	1.21		4.92	5.38	5.98
Sussex	1.02	1.11	1.21		4.71	5.11	5.57
Union	0.97	1.08	1.19		5.05	5.59	6.20
Warren	1.01	1.09	1.19		4.93	5.34	5.80

SEE EXCEL TABLES FOR CURRENT DATA TABLE D3. County-based 100-yr ARI change factors and projected precipitation estimates for 2020-2069 under RCP4.5 emissions.

County	Change Factor				Projected Precipitation		
	17th Percentile	Median	83rd Percentile		17th Percentile	Median	83rd Percentile
Atlantic	0.89	1.11	1.30		7.89	9.85	11.53
Bergen	0.94	1.12	1.33		7.87	9.39	11.14
Burlington	0.93	1.10	1.25		8.28	9.79	11.09
Camden	0.97	1.11	1.27		8.20	9.39	10.73
Cape May	0.90	1.12	1.27		7.73	9.60	10.94
Cumberland	0.84	1.07	1.28		7.33	9.36	11.18
Essex	0.93	1.10	1.32		8.05	9.56	11.47
Gloucester	0.95	1.10	1.26		8.13	9.42	10.79
Hudson	0.89	1.07	1.25		7.32	8.80	10.29
Hunterdon	0.93	1.11	1.33		7.44	8.95	10.73
Mercer	0.95	1.10	1.29		7.87	9.11	10.65
Middlesex	0.90	1.10	1.34		7.78	9.46	11.52
Monmouth	0.90	1.06	1.27		8.07	9.46	11.34
Morris	0.95	1.13	1.43		7.95	9.46	11.94
Ocean	0.93	1.07	1.23		8.65	9.90	11.37
Passaic	0.95	1.14	1.43		8.08	9.75	12.22
Salem	0.93	1.08	1.24		7.97	9.24	10.57
Somerset	0.93	1.14	1.44		7.55	9.21	11.64
Sussex	0.95	1.13	1.33		7.13	8.48	9.93
Union	0.93	1.10	1.35		8.09	9.62	11.73
Warren	0.91	1.10	1.24		7.11	8.58	9.70